

**Salt Dynamics in Well-Mixed Estuaries
Importance of Advection by Tides**

Wei, Xiaoyan; Schuttelaars, Henk; Schramkowski, George

DOI

[10.1175/JPO-D-15-0045.1](https://doi.org/10.1175/JPO-D-15-0045.1)

Publication date

2016

Document Version

Final published version

Published in

Journal of Physical Oceanography

Citation (APA)

Wei, X., Schuttelaars, H., & Schramkowski, G. (2016). Salt Dynamics in Well-Mixed Estuaries: Importance of Advection by Tides. *Journal of Physical Oceanography*, 46(5), 1457-1475. <https://doi.org/10.1175/JPO-D-15-0045.1>

Important note

To cite this publication, please use the final published version (if applicable).
Please check the document version above.

Copyright

Other than for strictly personal use, it is not permitted to download, forward or distribute the text or part of it, without the consent of the author(s) and/or copyright holder(s), unless the work is under an open content license such as Creative Commons.

Takedown policy

Please contact us and provide details if you believe this document breaches copyrights.
We will remove access to the work immediately and investigate your claim.

Salt Dynamics in Well-Mixed Estuaries: Importance of Advection by Tides

XIAOYAN WEI

Applied Mathematics, Delft University of Technology, Delft, Netherlands

GEORGE P. SCHRAMKOWSKI

Flanders Hydraulics Research, Antwerp, Belgium

HENK M. SCHUTTELAARS

Applied Mathematics, Delft University of Technology, Delft, Netherlands

(Manuscript received 19 February 2015, in final form 24 December 2015)

ABSTRACT

Understanding salt dynamics is important to adequately model salt intrusion, baroclinic forcing, and sediment transport. In this paper, the importance of the residual salt transport due to tidal advection in well-mixed tidal estuaries is studied. The water motion is resolved in a consistent way with a width-averaged analytical model, coupled to an advection–diffusion equation describing the salt dynamics. The residual salt balance obtained from the coupled model shows that the seaward salt transport driven by river discharge is balanced by the landward salt transport due to tidal advection and horizontal diffusion. It is found that the tidal advection behaves as a diffusion process, and this contribution is named tidal advective diffusion. The horizontal diffusion parameterizes processes not explicitly resolved in the model and is called the prescribed diffusion. The tidal advective diffusion results from the correlation between the tidal velocity and salinity and can be explicitly calculated with the dominant semidiurnal water motion. The sensitivity analysis shows that tidal advective diffusivity increases with increasing bed roughness and decreasing vertical eddy viscosity. Furthermore, tidal advective diffusivity reaches its maximum for moderate water depth and moderate convergence length. The relative importance of tidal advective diffusion is investigated using the residual salt balance, with the prescribed diffusion coefficient obtained from the measured salinity field. The tidal advective diffusion dominates the residual salt transport in the Scheldt estuary, and other processes significantly contribute to the residual salt transport in the Delaware estuary and the Columbia estuary.

1. Introduction

Both the spatial and temporal distribution of salinity can significantly influence residual water motion through the gravitational and tidal straining circulation (Burchard et al. 2011; Geyer and MacCready 2014). This affects both tidal and residual transport of sediment, pollutants, and other waterborne materials. Hence, a good understanding of salt dynamics is critical to simulating, forecasting, and controlling salt intrusion in estuaries, for example, to maintain sufficient freshwater intake in deltas.

The salinity structure in tidal estuaries is maintained by the competing influences of river flow, which tends to

drive saltwater seaward; the gravitational circulation, which tends to drive saltwater landward; and a down-gradient salt flux due to shear dispersion, tidal pumping, and other processes (MacCready 2004). To identify different driving mechanisms for the estuarine salt flux, many researchers decomposed the current and salinity fields (spatially and temporally) using both short-term and long-term time series of data (Fischer 1972; Hughes and Rattray 1980; Bowen and Geyer 2003; Lerczak et al. 2006). However, as the results strongly depend on the methods of decomposition (Rattray and Dworski 1980), it is difficult to get insights into the physical mechanisms resulting in the residual salt transport from various decomposition methods.

The pursuit of theoretically identifying transport processes in flow dates back to the 1950s (Taylor 1953, 1954), when Taylor resolved contaminant dispersion in a

Corresponding author address: Xiaoyan Wei, Delft University of Technology, Mekelweg 4, 2624 CD, Delft, Netherlands.
E-mail: xywei1988@hotmail.com

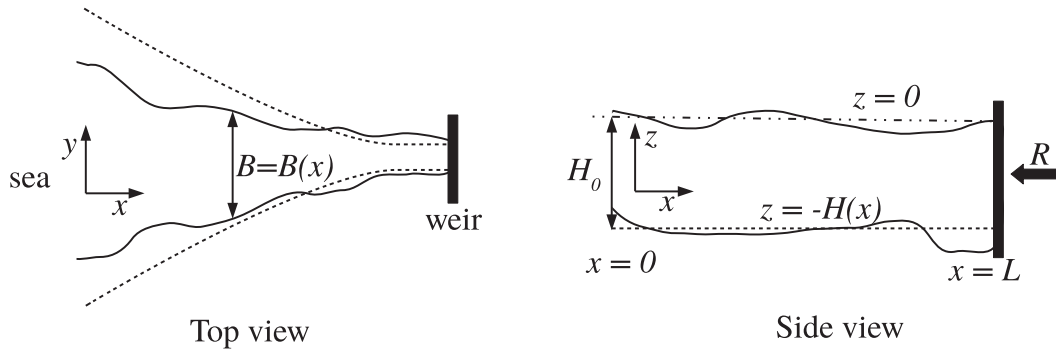


FIG. 1. The top view and the side view of the estuary, with x as the longitudinal coordinate positive in the landward direction, y as the transverse coordinate, and z as the vertical coordinate positive in the upward direction. Here, $H(x)$ is the water depth of the estuary and $B = B(x)$ is the estuarine width; H_0 is the estuarine depth at the mouth; and R is the river discharge from upstream. The dashed lines represent an estuary with an exponentially converging width and a horizontal bed, which is used for parameter sensitivity study.

straight circular tube under a steady pressure gradient. To identify the main salt transport processes in estuaries, many analytical models for salt transport have been developed (Hansen and Rattray 1965; MacCready 2004). After tidally averaging all the physical quantities, their model results highlight the significant contribution of gravitational circulation to residual salt transport. To resolve the tidal contribution to salt transport, McCarthy (1993) developed a coupled model of the tidal water motion and salinity at the tidal time scale for well-mixed estuaries. There, the residual salt transport due to river discharge is balanced by the transport resulting from tidal oscillatory dispersion and horizontal diffusive buoyancy transport.

In this paper, the salt dynamics in well-mixed estuaries will be investigated at the tidal time scale, extending the model from McCarthy (1993). We will focus on the tidal oscillatory dispersion contribution to the residual salt transport, which is parameterized as an along-channel diffusivity in classical theories (Geyer and MacCready 2014), and will be called the tidal advective diffusion in this paper. The main contribution of the paper is to show the sensitivity of the tidal advective diffusion to friction parameters and estuarine shape and its relative importance to the residual salt transport in real estuaries.

The paper is structured as follows: Section 2 introduces the width-averaged model, coupling hydrodynamics with salt dynamics. The solution method is introduced in section 3. Section 4 discusses the sensitivity of the tidal advective diffusivity to varying model parameters and estuarine geometry. The relative importance of tidal advection to the residual salt transport is studied for three estuaries: the Delaware estuary, the Scheldt estuary, and the Columbia estuary. In section 5, the sensitivity of the tidal advective diffusivity to model

parameters is explained and discussed, followed by a discussion of other important salt transport processes and the limitations of the model. Conclusions are drawn in section 6.

2. Model description

To investigate the residual, along-channel salt transport for estuaries that are tidally dominated and well-mixed, the approach taken by McCarthy (1993) is followed. However, a different expression for the tidal salinity component is obtained [see Eq. (15) and appendix C for details], a different seaward boundary condition is used, and a weir is prescribed at the landward side. Furthermore, the model is extended for estuaries with arbitrary depth and width (see Fig. 1).

The water motion is described by the width-averaged continuity equation and the longitudinal momentum equation:

$$\frac{\partial u}{\partial x} + \frac{\partial w}{\partial z} + \frac{1}{B} \frac{dB}{dx} u = 0, \quad \text{and} \quad (1)$$

$$\frac{\partial u}{\partial t} + u \frac{\partial u}{\partial x} + w \frac{\partial u}{\partial z} = -\frac{g}{\rho_c} \int_z^\eta \frac{\partial \rho}{\partial x} dz - g \frac{\partial \eta}{\partial x} + \frac{\partial}{\partial z} \left(A_v \frac{\partial u}{\partial z} \right). \quad (2)$$

Here, t denotes time, u and w denote the longitudinal and vertical velocity components, η is the free surface elevation, ρ_c is the background density taken to be 1000 kg m^{-3} , ρ is the along-channel density, g is the acceleration of gravity, and A_v is the vertical eddy viscosity, which is assumed to be constant both in time and space. Hence, the influence of tidal straining on tidal flow is assumed to be small (Cheng et al. 2010).

The boundary conditions at the free surface ($z = \eta$) are the kinematic and no stress boundary conditions:

$$w = \frac{\partial \eta}{\partial t} + u \frac{\partial \eta}{\partial x} \quad \text{and} \quad A_v \frac{\partial u}{\partial z} = 0. \quad (3)$$

At the bottom [$z = -H(x)$], the normal water flux vanishes:

$$w = -\frac{dH}{dx} u. \quad (4)$$

A partial-slip condition is prescribed using a linearized bed stress (Schramkowski and De Swart 2002; Chernetsky et al. 2010), defined at ~ 1 m, just above the real bed (Schramkowski et al. 2010):

$$A_v \frac{\partial u}{\partial z} = su, \quad (5)$$

where the slip parameter s , depending on the bed roughness, is assumed to be constant both in time and space. In general, s can vary from zero in frictionless cases (free slip) to large values in strongly frictional cases (no slip).

The water motion is driven by a prescribed semi-diurnal tidal elevation M_2 at the entrance ($x = 0$):

$$\eta(t, 0) = a_{M_2} \cos(\sigma t), \quad (6)$$

where a_{M_2} is the constant amplitude of the M_2 tidal constituent, and σ is the M_2 tidal frequency.

At the weir ($x = L$), a constant river discharge R is prescribed:

$$B(L) \int_{-H}^{\eta(t)} u(L, z, t) dz = -R. \quad (7)$$

The density ρ is assumed to depend only on salinity and follows from the linear equation of state $\rho = \rho_c(1 + \beta_s S)$, with $\beta_s = 7.6 \times 10^{-4} \text{psu}^{-1}$. Here, S is the width-averaged salinity that is obtained from solving

$$\begin{aligned} \frac{\partial S}{\partial t} + u \frac{\partial S}{\partial x} + w \frac{\partial S}{\partial z} \\ = \frac{\partial}{\partial x} \left(K_h \frac{\partial S}{\partial x} \right) + K_h \frac{1}{B} \frac{dB}{dx} \frac{\partial S}{\partial x} + \frac{\partial}{\partial z} \left(K_v \frac{\partial S}{\partial z} \right), \end{aligned} \quad (8)$$

with K_h and K_v as the longitudinal and vertical eddy diffusivity coefficients, respectively, both assumed to be constant in time and space. Furthermore, the vertical eddy diffusivity K_v is assumed to be equal to the vertical eddy viscosity A_v , which varies from small values in strongly stratified cases to large values in well-mixed cases.

Instead of prescribing a zero salinity gradient at the estuarine mouth as required by McCarthy (1993), the salinity at the estuarine mouth is prescribed to be a constant S_m in this model,

$$S = S_m \quad \text{at} \quad x = 0, \quad (9)$$

and it is required that the residual salt transport vanishes at the weir:

$$\overline{\int_{-H}^{\eta} \left(-uS + K_h \frac{\partial S}{\partial x} \right) dz} = 0 \quad \text{at} \quad x = L. \quad (10)$$

Here, the overbar ($\overline{\quad}$) indicates tidally averaged quantities. Furthermore, the salt flux through the sea surface and the bottom has to vanish:

$$K_v \frac{\partial S}{\partial z} \Big|_{z=\eta} = K_v \frac{\partial S}{\partial z} \Big|_{z=-H} = 0. \quad (11)$$

3. Perturbation method

The system of equations, given by Eqs. (1)–(11), will be solved using an asymptotic approximation of the physical variables with a small parameter ε , the ratio of the M_2 tidal amplitude, and the water depth at the estuarine entrance (McCarthy 1993; Chernetsky et al. 2010). In this procedure, a scaling analysis is first used to make the equations dimensionless. Next, the various terms in the governing equations are ordered with respect to ε . As a next step, the physical variables are asymptotically expanded in ε :

$$\Phi = \Phi_0 + \varepsilon \Phi_1 + \varepsilon^2 \Phi_2 + \dots \quad (12)$$

with Φ representing any of the physical variables (η , u , w , S). The subscript 0 denotes the leading order, 1 denotes the first order, and so on. Finally, terms of the same order in ε are collected in the dimensionless governing equations and are required to balance. This results in a system of equations at each order of ε (see appendix A for details).

To obtain the leading-order salinity distribution and assess the importance of residual salt transport by the tidal buoyancy contribution, the leading-order water motion has to be solved, together with the leading-order and first-order salinity equation, and the depth-integrated second-order salinity equation. The leading-order hydrodynamic equations and corresponding solutions for rectangular basins and exponentially convergent estuaries are presented by Ianniello (1979) and Chernetsky et al. (2010) and for estuaries with an arbitrary geometry in appendix B.

The salinity equation in leading order reads

$$\frac{\partial S_0}{\partial t} = K_v \frac{\partial}{\partial z} \left(\frac{\partial S_0}{\partial z} \right), \quad (13)$$

which, together with the boundary condition (11), yields a steady, vertically homogeneous unknown background salinity field $S_0 = S_0(x)$. Here, the leading-order salinity is taken to be real. This is different from McCarthy (1993), who allows the leading-order density field to be a complex quantity; for a discussion, see appendix C. The salinity equation at first order reads

$$\frac{\partial S_1}{\partial t} + u_0 \frac{dS_0}{dx} = K_v \frac{\partial^2 S_1}{\partial z^2}. \quad (14)$$

Since S_0 is a function of x only, the salinity at first-order S_1 can be written as

$$S_1 = \Re(\hat{S}_1 e^{i\sigma t}), \quad \text{with} \quad \hat{S}_1 = \frac{d\hat{\eta}_0}{dx} \frac{dS_0}{dx} S_z(x, z), \quad (15)$$

and \hat{S}_1 is the complex amplitude of the first-order salinity, and \Re means only the real part is used. Solutions of $S_z(x, z)$ can be obtained analytically from Eq. (14) for estuaries of any bathymetry $H(x)$ (see appendix C).

Finally, the tidally averaged and vertically integrated $O(\varepsilon^2)$ salinity equation is derived:

$$\begin{aligned} -\frac{d}{dx} B(x) \int_{-H(x)}^0 \overline{S_1 u_0} dz + \frac{d}{dx} B(x) \int_{-H(x)}^0 K_h \frac{dS_0}{dx} dz \\ = -R \frac{dS_0}{dx}. \end{aligned} \quad (16)$$

Given horizontal eddy diffusivity K_h , the only unknown in Eq. (16) is dS_0/dx . Thus, the tidally averaged salinity profile S_0 , consistent with the tidal motion, river discharge, and geometrical parameters can be obtained. Note that the contribution due to the width-averaged and depth-integrated exchange flow induced by gravitational circulation is resolved but absent in Eq. (16). This is because the width-averaged and depth-integrated residual Eulerian flow $\int_{-H}^0 \overline{u_1} dz$ (including gravitational circulation), together with the Stokes drift $\eta_0 u_0|_{z=0}$, equals the width-averaged river discharge $-R/B$ (McCarthy 1993). The insignificance of gravitational circulation in well-mixed systems is in agreement with MacCready and Geyer (2010) and has been observed in North Inlet in South Carolina, where almost no gravitational circulation is found by Kjerfve (1986).

Nevertheless, the absence of gravitational circulation in the width-averaged and depth-integrated residual salt balance in this model does not imply that gravitational circulation does not contribute to residual salt transport. In well-mixed estuaries, contributions of exchange flows due to gravitational circulation and other components of exchange flow components can result in a significant transport of salinity due to variations in the lateral

direction. In this model, these contributions are not resolved explicitly but parameterized in the prescribed diffusion.

By substituting the solutions for S_1 and u_0 into (16), we find that

$$\begin{aligned} \frac{d}{dx} B(x) \left\{ \left[-\frac{1}{2} \Re \left(\int_{-H(x)}^0 \hat{S}_1 \hat{u}_0^* dz \right) \left(\frac{dS_0}{dx} \right)^{-1} \right. \right. \\ \left. \left. + K_h H(x) \right] \frac{dS_0}{dx} \right\} = -R \frac{dS_0}{dx}, \end{aligned} \quad (17)$$

with \hat{u}_0^* as the complex conjugate of \hat{u}_0 . Integrating Eq. (17) with respect to x , and using the condition that no net residual salt transport is allowed at the weir, we find that

$$(K_h^{\text{adv}} + K_h) \frac{dS_0}{dx} = -\frac{R}{H(x)B(x)} S_0. \quad (18)$$

The tidally averaged transport of salinity by tidal advection behaves as a diffusive process, with K_h^{adv} the corresponding diffusivity coefficient given by

$$K_h^{\text{adv}} = -\frac{1}{2} \Re \left[\frac{1}{H(x)} \int_{-H}^0 \hat{S}_1 \hat{u}_0^* dz \right] \left(\frac{dS_0}{dx} \right)^{-1}. \quad (19)$$

Hereinafter, we will call this diffusive contribution tidal advective diffusion. The diffusion contribution parameterized by the horizontal eddy diffusivity K_h will be called the prescribed diffusion. The tidal advective diffusivity K_h^{adv} measures the contribution of residual salt transport due to tidal advective diffusion, called the tidal buoyancy contribution by McCarthy (1993). Equation (19) shows that the tidal advective diffusion originates from the temporal correlation between the tidal velocity and salinity and can be calculated explicitly with given M_2 tidal information only. On the other hand, K_h is necessary to parameterize all unresolved processes of residual salt transport in the width-averaged model (the most important unresolved processes are discussed in section 5e). Since the processes are not resolved, K_h has to be prescribed. After solving (18), the leading-order salinity is easily obtained as

$$S_0(x) = S_m e^{-\int_0^x f_s dx}, \quad \text{with} \quad f_s = \frac{R}{H(x)B(x)} \frac{1}{K_h + K_h^{\text{adv}}}. \quad (20)$$

4. Results

Substituting the solutions of u_0 and S_1 [see Eqs. (C4) and (C5)] into Eq. (19) yields

$$K_h^{\text{adv}} = -\frac{1}{2} \Re \left\{ \frac{1}{H(x)} \left| \frac{d\hat{\eta}_0}{dx} \right|^2 \int_{-H(x)}^0 S_z(x, z) U^*(x, z) dz \right\}. \quad (21)$$

Equation (21) suggests that K_h^{adv} is proportional to $|d\hat{\eta}_0/dx|$ squared, which is proportional to a_{M_2} [see Eq. (B11)] and is independent of river discharge. The dependence of K_h^{adv} on the slip parameter s , vertical eddy viscosity and diffusivity A_v , estuarine depth H , and convergence length L_b is more complex, as can be seen from Eqs. (C4), (B11), and (C8). Therefore, the sensitivity of K_h^{adv} to s , A_v , H , and L_b are investigated in section 4a. In section 4b, the importance of tidal advective diffusion to residual salt transport is studied using field data for three different estuaries, that is, the Delaware estuary, the Scheldt estuary, and the Columbia estuary. To justify the well-mixed assumption, the relative difference of the top–bottom salinity is required to be at most of order ε in the region of salt intrusion: $\Delta S/S_{\text{bottom}} \leq O(\varepsilon)$. The Delaware estuary is considered to be well mixed because the vertical difference of salinity is much smaller than the salinity at the bottom in most of the salt intrusion region (Garvine et al. 1992). The Scheldt estuary is well mixed especially in the seaward part, with only a small local vertical salinity gradient (Peters and Wollast 1976). The stratification in the Columbia estuary is weak in the studied period of 24–26 October in 1980 during spring tide with low river discharge (Jay and Smith 1990c). These three different estuaries are also representative of systems with different bathymetric and geometric profiles. The geometry of the Delaware estuary can be approximated with a horizontal bed and an exponentially varying width with a constant convergence length. The geometry of the Scheldt estuary can be captured by splitting the estuary into two sections using a different convergence length per section, along with significant bathymetric variations

TABLE 1. Default values of model parameters.

Variables	a_{M_2}	L	H	L_b	s	A_v
Units	m	km	m	km	m s^{-1}	$\text{m}^2 \text{s}^{-1}$
Values	2	200	10	50	0.0099	0.0085

along the channel. In contrast, both the geometry and bathymetry of the Columbia estuary show complex variations.

a. Parameter sensitivities

In this section, we focus on idealized estuaries with a horizontal bed and an exponentially decreasing width (see dashed lines in Fig. 1), which is given by

$$B(x) = B_0 e^{-x/L_b}, \quad (22)$$

with B_0 as the estuarine width at the entrance, and L_b as the estuarine convergence length. The term L_b represents the along-channel change of the estuarine geometry; small values of L_b correspond to strongly convergent estuaries, while for very large L_b , the estuary becomes prismatic. The default parameter values for the sensitivity analysis are representative for the Scheldt estuary [see section 4b(2)], as listed in Table 1.

1) SENSITIVITY OF K_h^{adv} TO s AND A_v

In Fig. 2a, the sensitivity of K_h^{adv} to the slip parameter s is shown. It reveals that when increasing s from 0.0001 to 0.1 m s^{-1} , K_h^{adv} increases from almost zero to more than $100 \text{ m}^2 \text{ s}^{-1}$, and K_h^{adv} becomes almost independent of s for large values of s .

The term K_h^{adv} is very sensitive to the vertical eddy viscosity A_v , as shown in Fig. 2b. The largest value of K_h^{adv} ($\sim 4 \times 10^4 \text{ m}^2 \text{ s}^{-1}$) is found when A_v is about $10^{-3} \text{ m}^2 \text{ s}^{-1}$, while K_h^{adv} is much smaller ($K_h^{\text{adv}} \sim 10^2 \text{ m}^2 \text{ s}^{-1}$) for default A_v (see the dashed line in

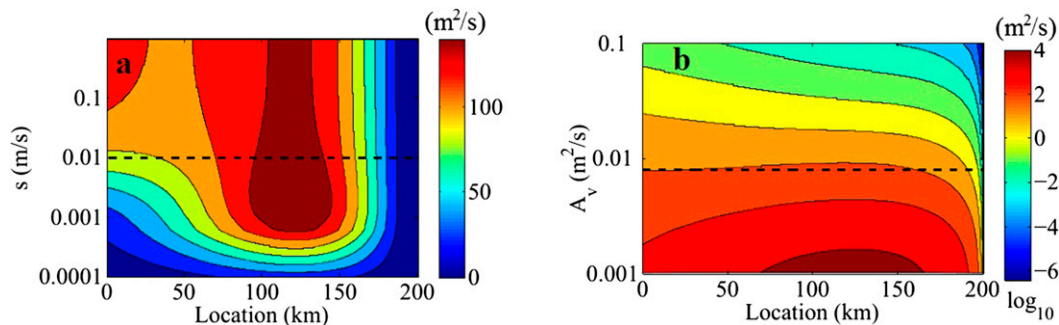


FIG. 2. The value of K_h^{adv} with varying (a) s and (b) A_v . Here, the dashed lines represent the default values for the slip parameter ($s = 0.0099 \text{ m s}^{-1}$) and vertical eddy viscosity ($A_v = 0.0085 \text{ m}^2 \text{ s}^{-1}$). The y axis is logarithmic in both figures.

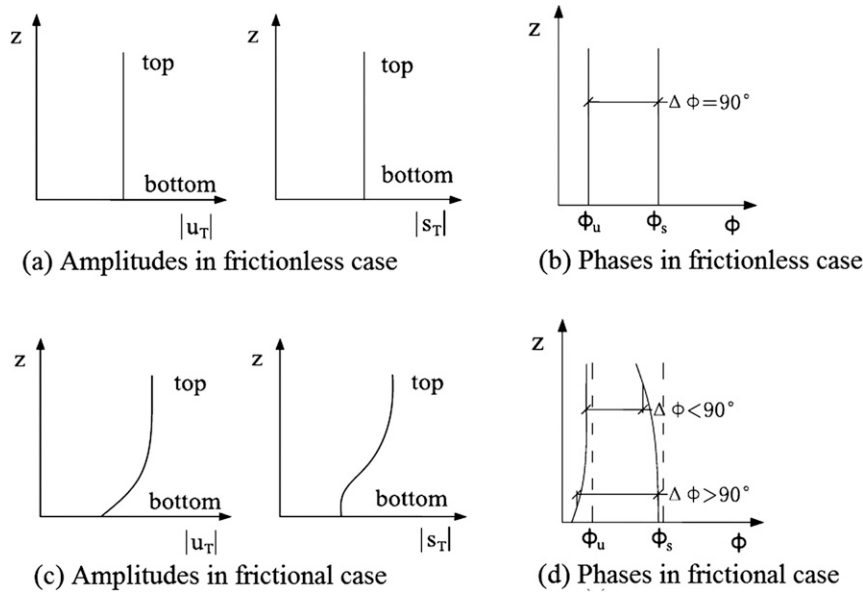


FIG. 3. The (left) amplitudes and (right) phases of the tidal velocity u_T and salinity s_T in (a),(b) frictionless and (c),(d) frictional cases. In this model, the M_2 tidal constituent is considered; hence, $u_T = u_0$ and $s_T = S_1$.

Fig. 2b). Larger values of A_v result in much smaller magnitudes of K_h^{adv} . Notice that this paper focuses on well-mixed estuaries; hence, A_v cannot be too small to ensure that the top to bottom salinity difference is not too large [$\Delta S/S_{\text{bottom}} \leq O(\epsilon)$]. Generally, the well-mixed assumption can be justified by requiring an approximate balance between the vertical mixing of salinity and its rate of change, as suggested by Eq. (13). Hence, A_v is constrained by $A_v/\sigma H_0^2 \geq O(1)$, scaling t and z with the tidal period σ^{-1} and the water depth H_0 , respectively. With the default values from Table 1, $A_v \geq 10^{-2} \text{ m}^2 \text{ s}^{-1}$ is required for the estuary to be well mixed.

To explain the observed parameter dependency, the residual salt flux due to tidal advective diffusion [hereinafter called the tidal advective salt flux (TASF)] is calculated for different s and A_v , using a constant residual salinity gradient of

$$\frac{dS_0}{dx} = -2 \times 10^{-4} \text{ psu m}^{-1}, \quad (23)$$

which is representative for the Scheldt estuary. TASF at a certain location (x, z) is given by

$$\frac{1}{2} \Re[\hat{S}_1(x, z) \hat{u}_0^*(x, z)] = \frac{1}{2} |\hat{S}_1| |\hat{u}_0| \cos(\phi_u - \phi_s). \quad (24)$$

Here, $S_1 = |\hat{S}_1| e^{-i\phi_s}$; $\hat{u}_0^* = |\hat{u}_0| e^{i\phi_u}$, with $|\cdot|$ as the absolute values of the tidal salinity S_1 and velocity u_0 ; and ϕ_u and

ϕ_s are the phases of the complex amplitudes of u_0 and S_1 . Equation (24) shows that TASF depends not only on the magnitudes of u_0 and S_1 , but also on their phase difference ($\Delta\phi = \phi_s - \phi_u$). Integrating TASF from the bottom to the top gives the residual tidal advective salt transport at location x . In case \hat{S}_1 and \hat{u}_0 are exactly out of phase ($\Delta\phi = 90^\circ$), there will be no residual salt transport due to tidal advective diffusion. This will be discussed in more detail in section 5.

In essence, TASF is resulting from the temporal correlation between u_0 and S_1 . In frictionless estuaries, the two-dimensional flow behaves like a one-dimensional flow (vertically uniform) with no turbulence/shear generated (see Figs. 3a,b). In this case, the peak tidal velocities proceed high S_1 and low S_1 by exactly 90° (see Fig. 3b), and no tidal advective salt transport is produced after one tidal cycle as the salt imported into the estuary during flood is exported out of the estuary during ebb. In (real) estuaries with bed friction, the bottom-induced turbulence is transferred throughout most of the water column, resulting in a vertically varying u_0 and S_1 (see Figs. 3c,d). In this case, the magnitude of u_0 near the top exceeds that near the bottom (see Fig. 3c) because water in the upper layers experiences less resistance from the bed friction. Meanwhile, the peak tidal velocities near the bottom lead those near the top (see Fig. 3d), owing to larger shear stress near the bottom. Therefore, since S_1 is mainly forced by u_0 as suggested by Eq. (14), S_1

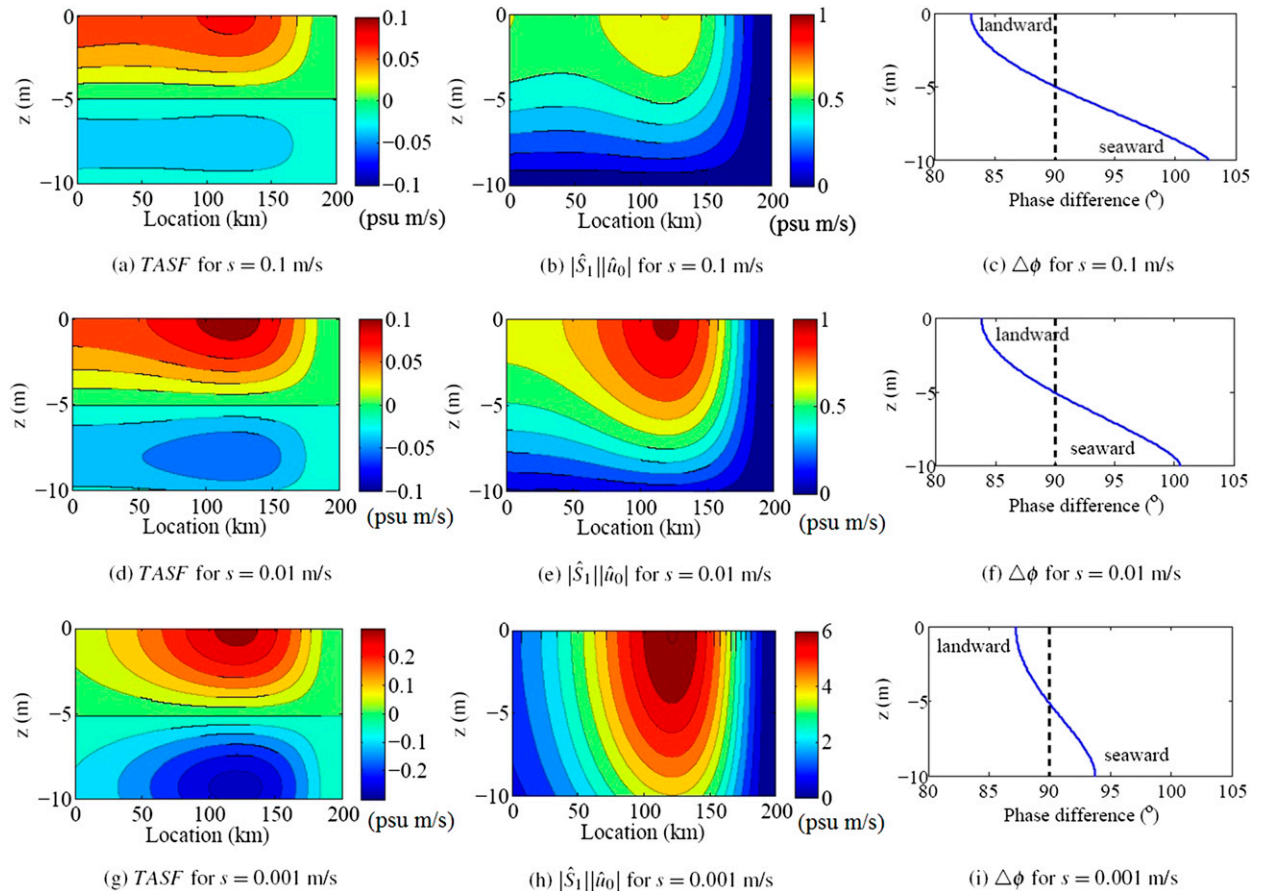


FIG. 4. TASF, $|\hat{S}_1||\hat{u}_0|$, and $\Delta\phi$ for different values of slip parameter s : (top) 0.1, (middle) 0.01, and (bottom) 0.001 m s^{-1} . Note that different color scales are used for TASF and $|\hat{S}_1||\hat{u}_0|$ for $s = 0.001 \text{ m s}^{-1}$. The dashed line in the right column shows the phase difference of $\Delta\phi = 90^\circ$.

becomes higher near the top than the bottom, and high S_1 at upper layers leads that at lower layers. As a result, S_1 slightly catches up with u_0 in the upper layer ($\Delta\phi < 90^\circ$), so that high S_1 coincides more with flood velocities and low S_1 coincides more with ebb velocities, resulting in a landward TASF in the upper layer. On the other hand, S_1 lags more behind u_0 in the lower layer ($\Delta\phi > 90^\circ$); thus, high S_1 coincides more with ebb velocities and low S_1 coincides more with flood velocities, resulting in a seaward TASF in the lower layer. Since the amplitudes of u_0 and S_1 are larger in the upper layers than the bottom, the landward TASF in upper layers exceeds the seaward TASF near the bottom, resulting in a net landward salt transport through the entire water column, namely, a landward tidal advective salt transport. This mechanism has been observed by [Bowen and Geyer \(2003\)](#).

(i) Slip parameter

In [Fig. 4](#) (left column), TASF throughout the estuary is shown for $s = 0.1, 0.01,$ and 0.001 m s^{-1} , respectively.

TASF is landward at the top and seaward at the bottom for all s . It means that tidal advective diffusion drives salt landward in the upper layer and transports salt seaward near the bottom. This result confirms the previous analysis and is consistent with the measurement in the Hudson estuary shown by [Bowen and Geyer \(2003\)](#), who found a landward oscillatory salt transport near the surface and seaward (or near zero) transport at the bottom.

The magnitude of TASF increases significantly when s decreases from 0.1 to 0.001 m s^{-1} . Concerning $|\hat{S}_1||\hat{u}_0|$, [Fig. 4](#) (middle column) shows its largest values are found near the surface, decreasing toward the bottom. With s decreasing from 0.1 to 0.001 m s^{-1} , $|\hat{S}_1||\hat{u}_0|$ increases at all depths and becomes vertically more homogeneous.

For estuaries with a horizontal bed and constant friction parameters, ϕ_u and ϕ_s are constant in the longitudinal direction; hence, $\Delta\phi$ only varies in the vertical direction. For all the three slip parameters, $\Delta\phi$ is smaller than 90° at the top and larger than 90°

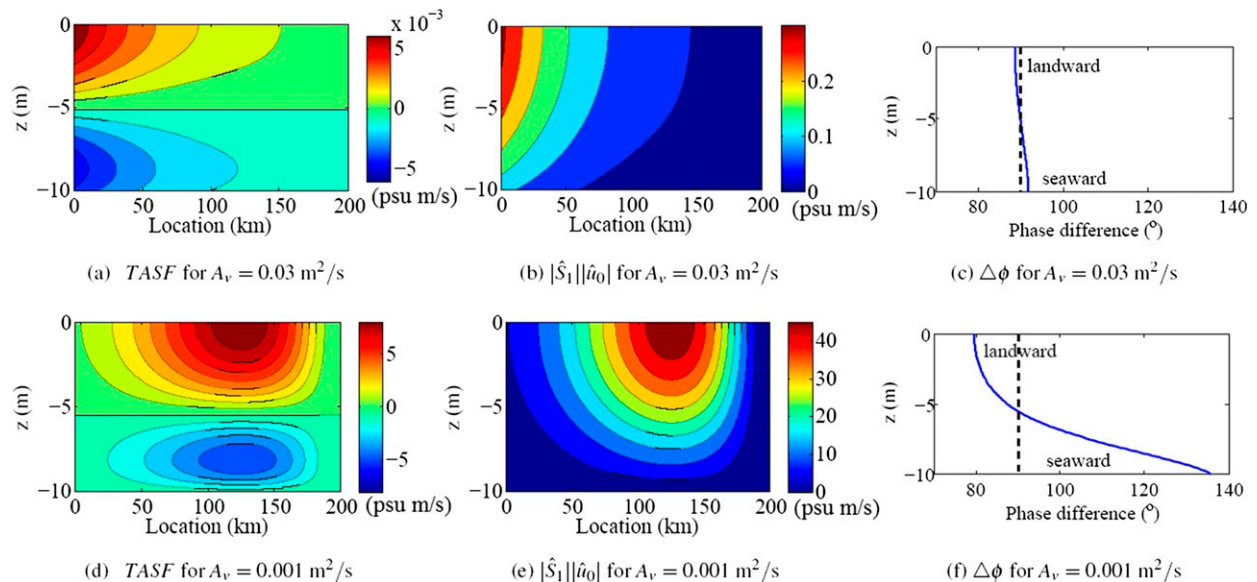


FIG. 5. TASF, $|\hat{S}_1||\hat{u}_0|$, and $\Delta\phi$ for different values of vertical eddy viscosity A_v : (a)–(c) 0.03 and (d)–(f) $0.001 \text{ m}^2 \text{ s}^{-1}$. Note the color scale differences used in (a), (b), and (d), (e), since TASF and $|\hat{S}_1||\hat{u}_0|$ change magnitude significantly with changing A_v .

near the bottom, consistent with Fig. 3d. This results in the landward tidal advective salt flux in the upper layer and seaward salt flux near the bottom. The right column of Fig. 4 also shows that $\Delta\phi$ becomes closer to 90° at all depths for decreasing s , with $\cos(\phi_u - \phi_s)$ being smaller. This observation, together with the fact that $|\hat{S}_1||\hat{u}_0|$ becomes more vertically uniform, leads to a smaller K_h^{adv} for decreasing s (see Fig. 2a), even though the magnitude of TASF increases for all depths.

(ii) Eddy viscosity

Figure 5 shows TASF, $|\hat{S}_1||\hat{u}_0|$, and $\Delta\phi$ for two different values of the vertical eddy viscosity: $A_v = 0.03$ and $0.001 \text{ m}^2 \text{ s}^{-1}$. TASF increases significantly when A_v decreases from 0.03 to $0.001 \text{ m}^2 \text{ s}^{-1}$ (see Fig. 5, left column). This increase corresponds well with the strong increase of K_h^{adv} (as seen in Fig. 2b). Figure 5, middle column, displays a strong increase in $|\hat{S}_1||\hat{u}_0|$ for decreasing A_v , with $|\hat{S}_1||\hat{u}_0|$ becoming less vertically homogeneous. Furthermore, the maximum values of $|\hat{S}_1||\hat{u}_0|$ move from the mouth to a more landward location; $\Delta\phi$ for different values of A_v is shown in the right column of Fig. 5. For $A_v = 0.03 \text{ m}^2 \text{ s}^{-1}$, $\Delta\phi$ is very close to 90° with a slight change from 89° at the top to 92° at the bottom. For $A_v = 0.001 \text{ m}^2 \text{ s}^{-1}$, $\Delta\phi$ strongly deviates from 90° , varying from 80° at the top to 135° at the bottom. The magnitude of $\cos(\phi_u - \phi_s)$ is much larger in the latter case. Therefore, the significant increase of K_h^{adv} for decreasing A_v is due to the overall effects of increasing

magnitude and larger vertical variations of $|\hat{S}_1||\hat{u}_0|$, together with the altered $\Delta\phi$.

2) SENSITIVITY OF K_h^{adv} TO H AND L_b

Since the water motion is strongly affected by estuarine geometry and bathymetry (Friedrichs and Aubrey 1994; Lanzoni and Seminara 1998; Prandle 2003), the sensitivity of K_h^{adv} to estuarine depth H and convergence length L_b is investigated.

The influence of H on K_h^{adv} is shown in Fig. 6a. The maximum values for K_h^{adv} are found in estuaries with $H \sim 16 \text{ m}$, and K_h^{adv} decreases sharply when estuaries become either deeper or shallower. In Fig. 6b, the influence of L_b on K_h^{adv} is shown. In most of the estuary, K_h^{adv} first increases when L_b decreases from 1000 to 40 km and then decreases when L_b is further decreased from 40 to 10 km . The change of K_h^{adv} with L_b is very gradual when L_b is larger than 100 km , while the change is dramatic when L_b is small. Near the estuarine mouth, K_h^{adv} monotonically decreases for decreasing L_b . Results in Fig. 6 suggest that K_h^{adv} is more sensitive to H than L_b .

It is found that TASF significantly decreases when the estuary becomes very deep, accompanied with a decreasing and vertically more uniform $|\hat{S}_1||\hat{u}_0|$ (plots not shown). Furthermore, $\Delta\phi$ strongly deviates from 90° in deep estuaries but very close to 90° in shallow estuaries. The estuarine convergence length L_b influences TASF only through the tidal amplitudes $|\hat{S}_1||\hat{u}_0|$, which increases with L_b until $L_b \sim 50 \text{ km}$ and then decreases for further increasing L_b . Meanwhile, $\Delta\phi$ does not change with L_b .

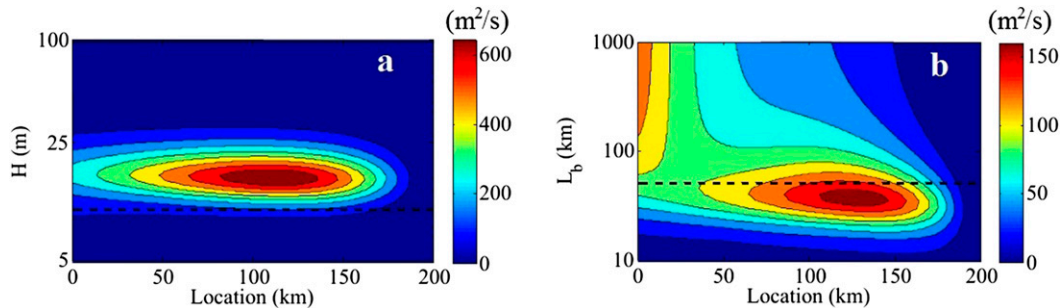


FIG. 6. The term K_h^{adv} with varying (a) H and (b) L_b . The y axis is logarithmic in both figures and the dashed lines show the default values of $H = 10$ m and $L_b = 50$ km.

b. Applications

As the tidal, advective, residual salt transport varies significantly with model parameters, its importance will be quantified for three estuaries: the Delaware, Scheldt, and Columbia. The length of these estuaries and their depth and width profiles are obtained from observations, as are the amplitude and phase of the M_2 sea surface elevation. The friction parameters s and A_v result from calibrating the M_2 sea surface elevation. To this end, the difference between the simulated and observed M_2 tidal elevation in the salt intrusion region is first evaluated using a cost function f based on least squares fit (Davies and Jones 1996)

$$f = \sum_{i=1}^{i=N} \sqrt{(\Delta\hat{\eta}_i)^2 + 2\hat{\eta}_i^{\text{obs}}\hat{\eta}_i^{\text{mod}}(1 - \cos\Delta\Phi_i)}, \quad (25)$$

with $\Delta\hat{\eta}_i = \hat{\eta}_i^{\text{obs}} - \hat{\eta}_i^{\text{mod}}$ and $\Delta\Phi_i = \Phi_i^{\text{obs}} - \Phi_i^{\text{mod}}$. Here, $\hat{\eta}_i^{\text{obs}}$ and Φ_i^{obs} are the observed M_2 tidal amplitude and phase, $\hat{\eta}_i^{\text{mod}}$ and Φ_i^{mod} are the simulated M_2 tidal amplitude and phase, and the subscript i indicates the numbering of the observed location. A range of A_v and s values are used in this procedure, with more than one combination of A_v and s producing approximately the same error close to the minimum. As a next step, different combinations of A_v and s values are used to plot the M_2 tidal elevation in the whole estuary, and the combination giving the best fit is selected (by visual inspection) as the final A_v and s values.

Then, using observed tidally averaged salinity profiles, the total diffusivity

$$K_h^{\text{total}} = K_h + K_h^{\text{adv}} \quad (26)$$

can be obtained by applying Eq. (18). Since K_h^{adv} can be explicitly calculated, K_h follows directly from $K_h = K_h^{\text{total}} - K_h^{\text{adv}}$. The ratio $r_s = K_h^{\text{adv}}/K_h^{\text{total}}$ quantifies the relative importance of the residual salt transport due to tidal advective diffusion.

1) THE DELAWARE ESTUARY

The geometry of the Delaware estuary can be approximated as an exponentially converging estuary with a constant convergence length of $L_b = 42$ km (with $B_0 = 39$ km) and a constant water depth (Kuijper and Van Rijn 2011; see blue lines in Fig. 7a). The tidal data of the Delaware estuary are taken from Friedrichs and Aubrey (1994). The salinity data for the central part (blue dots in Fig. 7b) are obtained from Kuijper and Van Rijn (2011), while the salinity at the entrance (blue dot circled by a red line in Fig. 7b) is taken from Garvine et al. (1992). Here, the salt intrusion length is about 150 km. The river discharge is $\sim 72 \text{ m}^3 \text{ s}^{-1}$ (Kuijper and Van Rijn 2011; Savenije 2012).

The constant water depth $H = 8$ m is chosen since it gives the best fit of the M_2 sea surface elevation compared to the observed data, together with a friction parameter setting of $s = 0.039 \text{ m s}^{-1}$ and $A_v = 0.005 \text{ m}^2 \text{ s}^{-1}$ (see Fig. 8a and Table 2). This constant water depth is considered as an effective water depth, which parameterizes unresolved processes like the lateral variations especially near the entrance; hence, it is different from the measured mean depth from Friedrichs and Aubrey (1994). In general, the M_2 tidal properties are well reproduced by the model, with almost constant M_2 tidal amplitude in the first 150 km and an amplification in the most landward part. The simulated M_2 phase corresponds well with the observed data throughout the Delaware estuary.

Using these observations, K_h^{adv} , K_h , and K_h^{total} are calculated within the region of salt intrusion ($x < 150$ km; see Fig. 8b). The term K_h^{adv} remains approximately $20 \text{ m}^2 \text{ s}^{-1}$ in the seaward reach and slightly increases to $\sim 30 \text{ m}^2 \text{ s}^{-1}$ in the central region. The term K_h first decreases from $\sim 180 \text{ m}^2 \text{ s}^{-1}$ at the mouth to $50 \text{ m}^2 \text{ s}^{-1}$ at $x = 80$ km. Next, it gradually increases to $\sim 70 \text{ m}^2 \text{ s}^{-1}$ in the landward direction. As a result, K_h^{total} decreases from $\sim 200 \text{ m}^2 \text{ s}^{-1}$ at the mouth to about $70 \text{ m}^2 \text{ s}^{-1}$ at $x = 80$ km and slightly increases landwards.

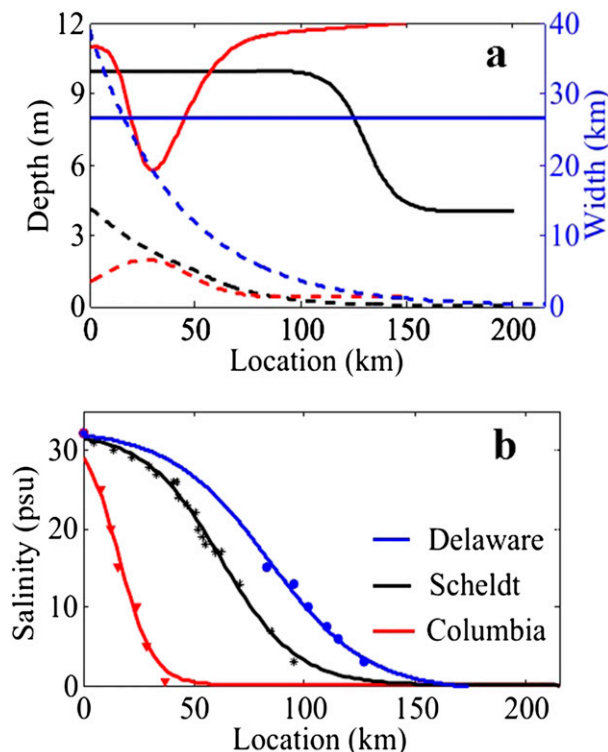


FIG. 7. (a) The geometry and bathymetry of the Delaware estuary (blue), Scheldt estuary (black), and Columbia estuary (red), with solid lines for water depth and dashed lines for estuarine width. (b) The observed residual salinity (dots) for the three estuaries, together with a fitted hyperbolic tangent profile of salinity for each (solid lines).

The ratio r_s increases from ~ 0.1 at the estuarine mouth to ~ 0.3 in the central region (see Fig. 8b). This suggests that in the central region of salt intrusion, tidal advective diffusion is an important process but not the dominant one for residual salt transport.

2) THE SCHELDT ESTUARY

The width of the Scheldt estuary can be described by two exponentially converging parts, with a convergence length of about 50 km in the downstream reach (up to 50 km from the mouth) and 28 km in the landward section of the estuary (Kuijper and Van Rijn 2011; see black dashed line in Fig. 7a). The water depth of the Scheldt estuary decreases from 10 m at the seaward side to less than 5 m at the landward side (Savenije and Veling 2005; see black solid line in Fig. 7a). The tidal data are taken from Savenije (1993), and the salinity data are from Kuijper and Van Rijn (2011), with a salt intrusion length of ~ 100 km (see black dots and line in Fig. 7b) for a river discharge of about $90 \text{ m}^3 \text{ s}^{-1}$ (Savenije 2012).

The M_2 sea surface elevation in the Scheldt estuary is best fitted with the observed data for $s = 0.0099 \text{ m s}^{-1}$

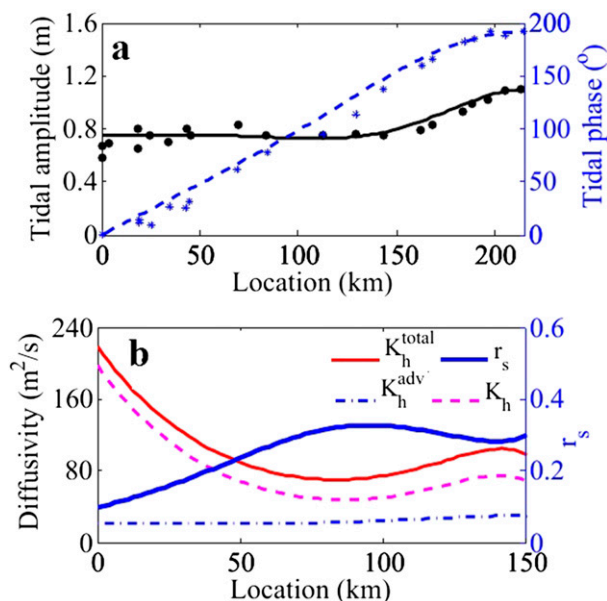


FIG. 8. (a) The modeled M_2 sea surface amplitude (black solid line) and phase (blue dashed line) vs the observed M_2 tidal surface amplitude (black dots) and phase (blue stars) in the Delaware estuary. (b) Diffusivity (K_h^{adv} , K_h , and K_h^{total}) and the ratio r_s in the region of salt intrusion.

and $A_v = 0.0085 \text{ m}^2 \text{ s}^{-1}$ (see Fig. 9a and Table 2). In general, the M_2 tidal properties are well reproduced by the model, with an amplification in the first 120 km and an abrupt damping in the landward part. The M_2 phase is slightly overestimated in the seaward part of the Scheldt estuary. Along the Scheldt estuary, K_h^{adv} remains around $\sim 10^2 \text{ m}^2 \text{ s}^{-1}$ in the region of salt intrusion ($x < 100$ km; see Fig. 9b). The highest K_h is found near the estuarine mouth ($K_h = 320 \text{ m}^2 \text{ s}^{-1}$). It significantly decreases to $\sim 10 \text{ m}^2 \text{ s}^{-1}$ at around $x = 60$ km and slightly increases again in the landward direction. The total diffusivity, therefore, decreases from more than $400 \text{ m}^2 \text{ s}^{-1}$ at the mouth to about $100 \text{ m}^2 \text{ s}^{-1}$ at $x = 50$ km and then increases gradually. As shown in Fig. 9b, the relative contribution of the tidal advective diffusion is higher than 0.50 (with a maximum of 0.7), except in the region close to the estuary mouth and near the end of the salt intrusion. Hence, tidal advective diffusion is a dominant

TABLE 2. Model parameters for each estuary from calibration of M_2 tidal data.

Variables	Units	Delaware	Scheldt	Columbia
a_{M_2}	m	0.75	2	2.05
L	km	215	200	150
R	$\text{m}^3 \text{ s}^{-1}$	72	90	3800
s	m s^{-1}	0.039	0.0099	0.035
A_v	$\text{m}^2 \text{ s}^{-1}$	0.0050	0.0085	0.0060

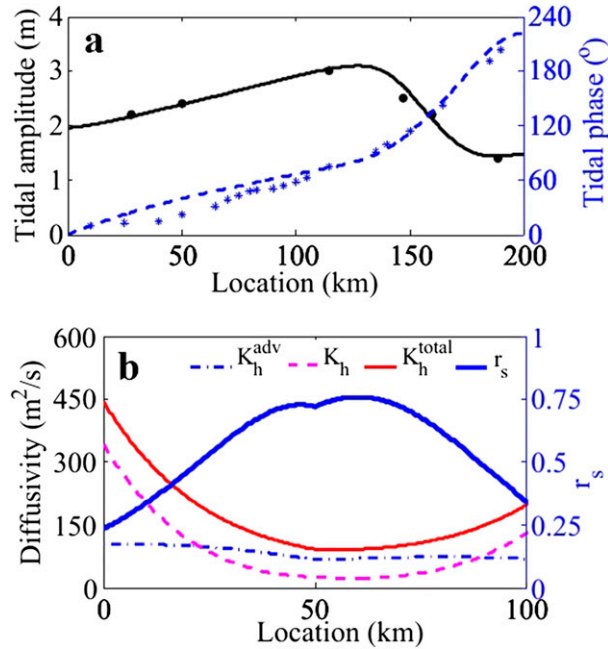


FIG. 9. As in Fig. 8, but for the Scheldt estuary.

process for residual salt transport in the central region of salt intrusion in the Scheldt estuary, whereas the contribution of all other parameterized processes is small.

3) THE COLUMBIA ESTUARY

For the Columbia estuary, the geometry and the tidal data are taken from Giese and Jay (1989). The width and depth of the Columbia estuary is highly variable (see red lines in Fig. 7a). The salt intrusion length is about 50 km (see red dots and line in Fig. 7b) according to the observations from Jay and Smith (1990c), using a low river discharge of $\sim 3800 \text{ m}^3 \text{ s}^{-1}$.

The M_2 sea surface elevation is best matched by the model for $s = 0.035 \text{ m s}^{-1}$ and $A_v = 0.006 \text{ m}^2 \text{ s}^{-1}$ (see Fig. 10a and Table 2). The M_2 tidal amplitude is reasonably well reproduced while the M_2 phase is slightly underestimated in the landward part of the Columbia estuary. It implies the friction in the landward part of the estuary is underestimated. However, the general M_2 tidal properties are well reproduced, with a slight increase of the M_2 tide in the first 10 km and a consistent decrease afterward.

Giese and Jay (1989) show that in the Columbia estuary, tidal constituents of S_2 , K_1 , O_1 , P_1 , and N_2 are all nonnegligible compared to M_2 , even though the M_2 tidal constituent is the most significant one. Here, all these contributions are included by linearly adding up their tidal amplitudes, resulting in an equivalent tidal amplitude $a_{M_2}^{eqv}$. The equivalent tidal frequency is taken to be the M_2 tidal frequency. An equivalent tidal amplitude at

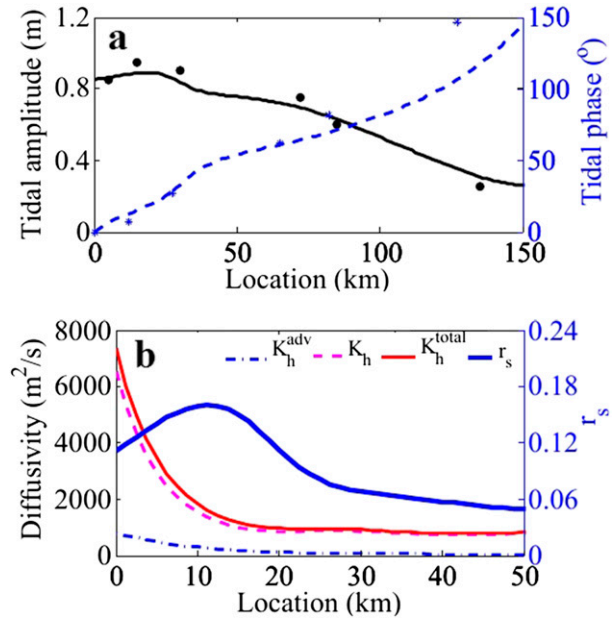


FIG. 10. As in Fig. 8, but for the the Columbia estuary.

the entrance $a_{M_2}^{eqv} = 2.05 \text{ m}$ is used to quantify the salt transport contribution of tidal advective diffusion for the Columbia estuary, according to a 1-yr record by Giese and Jay (1989).

The three diffusion coefficients, K_h^{adv} , K_h and K_h^{total} , and the ratio r_s are shown in Fig. 10b. Diffusion K_h^{adv} varies from $800 \text{ m}^2 \text{ s}^{-1}$ at the mouth to $50 \text{ m}^2 \text{ s}^{-1}$ at the end of salt intrusion; K_h decreases from 6500 to $850 \text{ m}^2 \text{ s}^{-1}$. As a result, K_h^{total} drops from about $7000 \text{ m}^2 \text{ s}^{-1}$ at the mouth to about $900 \text{ m}^2 \text{ s}^{-1}$ at the end of salt intrusion; K_h^{adv} is very small compared to K_h . The relative contribution of the tidal advective diffusion r_s is approximately 0.16 at about $x = 10 \text{ km}$, which is close to the result of Hughes and Rattray (1980). They found that the $\bar{A}(u_0 S_1)$ is about 0.22 of the total salt transport processes at the Clatsop Spit section ($\sim 10 \text{ km}$ away from the estuary mouth) during low discharge. Here, u_0 and S_1 are the cross-sectionally averaged tidal velocity and salinity, and \bar{A} is the tidally averaged area of the cross section. The relatively low magnitude of r_s suggests that the lateral processes and lateral variations of longitudinal processes parameterized in the present model are significant in the Columbia estuary.

5. Discussion

It has been found that the effect of salinity transport by tidal advection acts as a horizontal diffusive process with a diffusivity K_h^{adv} . This diffusivity is similar to the virtual coefficient of diffusion obtained in the classical

work by Taylor (1953, 1954). The similarity arises because the cross-sectional mixing time is short, and the effect of horizontal diffusivity is small compared to vertical diffusivity.

The values of A_v obtained for the three estuaries are much smaller than the approximated value using a simple boundary layer approximation for a well-mixed system: $A_v \sim \kappa \sqrt{su}(z + H + z_0)$, with κ the Von Kármán constant and z_0 the roughness height. This deviation can be explained by the procedure for calibrating the M_2 tidal surface elevation. As mentioned previously, A_v and s for a real estuary are chosen by minimizing the difference between the simulated and observed M_2 tidal elevation. However, in reality, the observed M_2 tidal elevation is affected by many factors such as wind, lateral processes, asymmetric mixing, and the nonlinear impact of higher harmonics (Jones and Davies 1996), which are not considered in the present width-averaged model. Hence, A_v and s obtained from the calibration procedures are actually effective vertical eddy viscosity and slip parameters, parameterizing all processes unresolved in the model, and they cannot be directly related using the above-mentioned simple boundary layer approximation.

In this section, the sensitivity of K_h^{adv} to model parameters will be explained by making an estimate of its magnitude in terms of dimensionless parameters. Substituting the tidal velocity and salinity into Eq. (19) yields an estimate of K_h^{adv} (see details in appendix D):

$$K_h^{\text{adv}} \approx \frac{8}{945} \frac{g^2}{\sigma^3} \left| \frac{d\hat{\eta}_0}{dx} \right|^2 |\alpha|^2 \frac{1}{\text{Stk}^6}, \quad (27)$$

$$\text{with } \alpha = \left[\cosh(\delta) + \frac{i}{\delta s^*} \sinh(\delta) \right]^{-1}, \quad s^* = \frac{s}{\sigma H},$$

$$\delta = (1 + i)/\text{Stk} \quad \text{and} \quad \text{Stk} = \sqrt{\frac{2A_v}{\sigma H^2}}.$$

The term Stk is the Stokes number, defined as the ratio of the frictional depth to the water depth (Souza 2013). Equation (27) is derived by assuming a small $|\delta|$ ($< \sqrt{2}$) for well-mixed systems (see appendix D for detail). This equation suggests that K_h^{adv} can be directly estimated using the M_2 sea surface gradient, the effective turbulence, and friction parameters. The term K_h^{adv} is proportional to the M_2 sea surface gradient squared, and it is affected by the Stokes number and the dimensionless slip parameter s^* .

To calculate the estimated K_h^{adv} , the sea surface elevation is first calibrated to obtain the effective s and A_v for each estuary. Then, the parameters α and Stk at every longitudinal position can be calculated using the

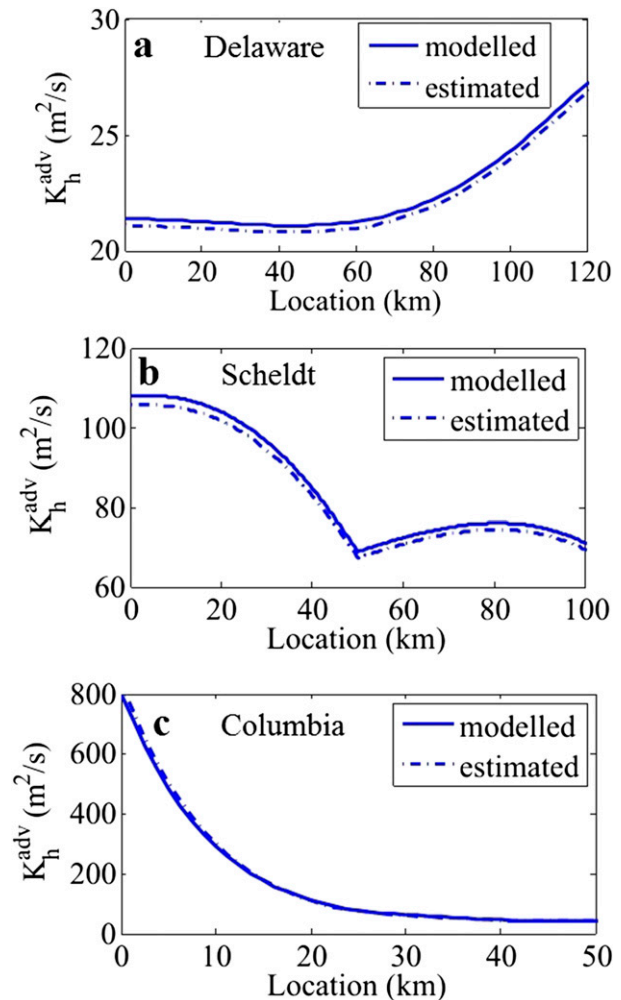


FIG. 11. The comparison of K_h^{adv} from the model (solid lines) with the estimated K_h^{adv} using Eq. (27) (dashed-dotted lines) for the (a) Delaware estuary, (b) Scheldt estuary, and (c) Columbia estuary.

bathymetry profiles of the three estuaries from section 4b. After that, the estimated K_h^{adv} at every location of each estuary can be obtained from Eq. (27). The accuracy of this estimate is shown in Fig. 11, where the analytical solution of K_h^{adv} evaluated from Eq. (19) is compared with the estimated K_h^{adv} for the Delaware estuary, the Scheldt estuary, and the Columbia estuary. In general, the estimated values agree well with the analytical solutions, with less than 5% difference between them for all three estuaries. It indicates that Eq. (27) is indeed a good estimate of K_h^{adv} , both for estuaries with a horizontal bed and those with nonuniform bathymetry. With this estimate of K_h^{adv} , the sensitivity of K_h^{adv} to the dimensionless slip parameter, the Stokes number, estuarine depth, and convergence length can be explained.

a. Influence of the dimensionless slip parameter

The dimensionless slip parameter s^* affects K_h^{adv} mainly through the parameter α , while the influence of s^* through the sea surface gradient is minor. For large values of s^* , approaching a no-slip boundary condition, α goes to $1/\cosh(\delta)$. This implies that increasing s^* further does not change K_h^{adv} since the flow hardly changes when s^* goes to infinity. On the other hand, for very small values of s^* , a free-slip condition is approximated and α becomes proportional to s^* . In this case, K_h^{adv} goes to zero as s^* goes to zero. For s^* between these two limits, increasing s^* will increase α [see Eq. (D3)], resulting in an increase of K_h^{adv} , as observed in Fig. 2a.

b. Influence of the Stokes number

The Stokes number Stk describes the effect of bottom layer turbulence on the vertical structure of u_0 and S_1 (Souza 2013). Equation (27) shows K_h^{adv} is proportional to Stk^{-6} , which partly explains the strong sensitivity of K_h^{adv} on A_v .

Apart from the proportionality of K_h^{adv} to Stk^{-6} , Stk also affects K_h^{adv} through α and the sea surface gradient. The influence of Stk on α can be clearly seen by taking s^* to be large, but δ not too small, in which case α can be approximated as $1/\cosh(\delta)$. However, for small δ , Stk hardly affects α ; α only depends on the dimensionless slip parameter as $s^*/(s^* + i)$. The influence of Stk on the sea surface gradient, however, is only through affecting the complex wavenumber [see Eq. (B11) in appendix B]. For both large and small values of δ , the wavenumber is hardly depending on δ and hence independent of Stk . Since we focus on relatively small values of δ for well-mixed estuaries, the influence of K_h^{adv} through α and the sea surface gradient is smaller than that through Stk^{-6} .

c. Influence of estuarine depth

The influence of H on K_h^{adv} can be explained using Stk and s^* . When a shallow estuary becomes moderately deep (H varies from 5 to 16 m), the increase of depth results in a decrease of Stk and a strong increase of K_h^{adv} (see Fig. 6a). However, when the estuary becomes much deeper ($|\delta| \gg \sqrt{2}$), the dependency of K_h^{adv} on Stk^{-6} is no longer valid, increasing H is equivalent to decreasing s^* . In this case, u_0 and S_1 become almost uniform in the vertical ($\alpha \rightarrow 0$), and K_h^{adv} goes to zero.

d. Influence of the estuarine convergence length

From Eq. (27) it follows that the estuarine convergence length L_b influences K_h^{adv} only through altering the sea surface gradient. To better understand this influence, an asymptotic solution for the sea surface gradient is obtained for both very weakly converging and

very strongly converging estuaries, using analytical solutions for estuaries with a horizontal bed (see appendix B for these solutions).

For weakly converging estuaries (L_b is large), the sea surface gradient is approximately given by

$$\frac{d\hat{\eta}_0}{dx} \approx a_{M_2} e^{x/(2L_b)} \frac{k_0}{2} \frac{\sinh\left[\frac{k_0}{2}(x-L)\right]}{\cosh\left(\frac{k_0 L}{2}\right)}, \quad (28)$$

with $k_0 = \sqrt{4\sigma^2\delta/[gH(\alpha \sinh\delta - \delta)]}$ as the complex wavenumber for large values of L_b . In this case, the sea surface gradient exponentially decreases with L_b , which results in the significant decrease of K_h^{adv} when L_b increases from 40 to 1000 km, as shown in Fig. 6b. However, for very strongly convergent estuaries, the sea surface gradient is approximately given by

$$\frac{d\hat{\eta}_0}{dx} \approx a_{M_2} \frac{k_0^2 L_b}{2}. \quad (29)$$

Hence, the sea surface gradient linearly decreases with L_b ; thus, K_h^{adv} is decreasing for L_b varying from 40 to 10 km. Near the estuarine mouth, K_h^{adv} consistently decreases with L_b as the sea surface gradient near the mouth decreases for L_b varying from 1000 to 10 km.

e. Other salt transport mechanisms

The estuarine circulation due to density-driven/gravitational circulation (Hansen and Rattray 1965; MacCready 2004) and tidal straining (Burchard and Hetland 2010) is another important salt transport process. Gravitational circulation dominates the estuarine circulation in many (classical) estuaries and is usually much more significant in strongly stratified cases than in the weakly/partially mixed estuaries (Jay and Smith 1990a). In partially mixed and weakly stratified estuaries, the exchange flow is dominated by tidal straining (Burchard and Baumert 1998; Burchard et al. 2011). Besides estuarine circulation, there are other significant salt transport processes: lateral advection of the longitudinal momentum (Lerczak et al. 2006); tidal advective diffusion due to temporal correlation between the tidally varying velocity and salinity, also known as tidal oscillatory transport (Bowen and Geyer 2003); and the correlations between the tidal velocity and salinity and the tidal variation of the cross-sectional area (Hughes and Rattray 1980). In partially mixed systems like the Hudson estuary, the estuarine salt transport (induced by estuarine circulation) dominates over the tidal oscillatory transport. Contrary to estuaries with pronounced vertical stratification, estuarine salt transport can be negligible in weakly stratified or well-mixed estuaries

(Jay and Smith 1990b). In the North Inlet (Kjerfve 1986), for instance, the landward salt transport mainly results from the correlation between the tidally varying velocity, salinity, and water depth. Instead of calculating each of these processes explicitly, the present width-averaged model resolves only the width-averaged tidal advective diffusion while parameterizing all other processes in the prescribed diffusivity.

f. Model limitations

Many processes such as lateral processes and tidal straining are not taken into account in the present model. By using a constant eddy viscosity, the asymmetric tidal mixing (tidal straining) is assumed to be very small, though tidal mixing is usually larger during spring tide than neap tide in real estuaries, potentially affecting the tidal velocity and salinity. It means that significant asymmetric tidal mixing can result in a different salt transport contribution induced by tidal advective diffusion. Moreover, by taking a constant partial-slip parameter, the model excludes the influence of local bed friction variations on water motion and salt dynamics. More importantly, by neglecting the lateral processes that can be significant in well-mixed estuaries such as the Delaware estuary (Aristizábal and Chant 2013), gravitational circulation drops out from the main residual salt balance cross section. Therefore, to investigate the full salt dynamics using the model developed in this paper, the model is preferably applied to well-mixed, tidally dominated estuaries where lateral processes and tidal straining are not significant. However, in other estuaries where the above-mentioned conditions are not exactly satisfied, the present model can be used to estimate the salt transport contribution due to the width-averaged tidal advective diffusion.

6. Conclusions

The importance of tidal advective diffusion on the residual salt transport in well-mixed estuaries is studied by coupling the width-averaged, shallow-water equation and the salinity equation in a consistent way. This coupled system of equations is solved using a perturbation method, in which the physical quantities are expanded in a small parameter: the ratio of the M_2 tidal amplitude to the water depth at the estuarine mouth. The salt balance equation shows that the seaward residual salt transport driven by river discharge is balanced by the landward salt transport due to tidal advection and diffusive processes, which parameterizes unresolved processes. It is found that the salt transport due to tidal advection behaves effectively as a diffusive term. Therefore, we use the term tidal advective diffusion for

this contribution. The tidal advective diffusion results from the temporal correlation between the tidal velocity and salinity and can be calculated explicitly after solving the tidal water motion.

For estuaries in which the water motion is mainly forced by a M_2 tidal constituent, the tidal advective diffusivity is calculated after calibrating the M_2 tidal data using the partial-slip parameter and the vertical eddy viscosity. Sensitivity analysis shows that the tidal advective diffusivity increases with the increasing slip parameter, decreasing vertical eddy viscosity, and it reaches its maximum for moderate water depth and moderate convergence length. To understand this sensitivity, an estimate of the tidal advective diffusivity is made. This estimate reveals that the tidal advective diffusivity is proportional to the amplitude of the sea surface gradient squared, and it depends on the Stokes number and the dimensionless slip parameter. Results show that the influences of slip parameter and eddy viscosity on the tidal advective diffusivity are mainly through the parameter α and the Stokes number, with the influence of the Stokes number being more significant. The estuarine depth influences the tidal advective diffusivity through both changing the dimensionless slip parameter and Stokes number, while the influence of the estuarine convergence length on the tidal advective diffusivity is only through altering the along-channel sea surface gradient. Furthermore, tidal advective diffusion transports salt landward near the surface and seaward near the bottom, with the tidal advective transport over the complete water column being always nonnegative.

Using the residual salt balance, the prescribed diffusivity is obtained from the measured salinity field. The relative importance of the tidal advective diffusion is quantified for three estuaries: the Delaware estuary, the Scheldt estuary, and the Columbia estuary. The tidal advective diffusion dominates the residual salt transport processes in the central part of the Scheldt estuary, where up to 70% of the total residual salt transport is attributed to this process. In the Delaware estuary and the Columbia estuary, tidal advective diffusion contributes up to 30% and 16% to the total residual salt transport respectively. It suggests that the width-averaged tidal advective diffusion is less important than other processes such as lateral processes in the Delaware estuary and the Columbia estuary.

Acknowledgments. This research was supported by the China Scholarship Council (File 201206710049). The two anonymous reviewers are appreciated for their valuable comments, which greatly helped to improve the paper.

TABLE A1. Scales of physical variables.

Variable	Typical scale	Symbol	Expression
t	M_2 tidal frequency	σ	$\sigma^{-1}\tilde{t}$
η	M_2 tidal amplitude	a_{M_2}	$a_{M_2}\tilde{\eta}$
x	Estuarine length	L	$L\tilde{x}$
z	Water depth at mouth	H_0	$H_0\tilde{z}$
H	Water depth at mouth	H_0	$H_0\tilde{H}$
B	Estuarine width at mouth	B_0	$B_0\tilde{B}$
u	See Chernetsky et al. (2010)	$U = (\sigma a_{M_2} L)/H$	$U\tilde{u}$
w	See Chernetsky et al. (2010)	$W = (H_0/L)U$	$W\tilde{w}$
S	Salinity at mouth	S_m	$S_m\tilde{S}$

APPENDIX A

Scaling Analysis

A perturbation method is used to analytically solve Eqs. (1)–(11). First of all, variables are scaled with their typical scales (see Table A1), where dimensionless variables are denoted by a tilde ($\tilde{\cdot}$). The density gradient scale is taken as the density difference between the seaward and landward side (McCarthy 1993) divided by the estuarine length, ($\Delta\rho = \rho_s - \rho_r$)/ L , with ρ_s and ρ_r as the density of seawater and river flow. The dimensionless water motion equations read

$$\frac{\partial\tilde{u}}{\partial\tilde{x}} + \frac{\partial\tilde{w}}{\partial\tilde{z}} + \frac{1}{\tilde{B}} \frac{d\tilde{B}}{d\tilde{x}} \tilde{u} = 0, \quad \text{and} \quad (\text{A1})$$

$$\begin{aligned} \frac{\partial\tilde{u}}{\partial\tilde{t}} + \frac{U}{\sigma L} \tilde{u} \frac{\partial\tilde{u}}{\partial\tilde{x}} + \frac{U}{\sigma L} \tilde{w} \frac{\partial\tilde{u}}{\partial\tilde{z}} = \frac{\Delta\rho H_0}{U\sigma L} \frac{g}{\rho_c} \frac{\partial\tilde{p}}{\partial\tilde{x}} \left(\tilde{z} - \frac{a_{M_2}}{H_0} \tilde{\eta} \right) \\ - \frac{a_{M_2}}{U\sigma L} g \frac{\partial\tilde{\eta}}{\partial\tilde{x}} + \frac{A_v}{\sigma H_0^2} \frac{\partial^2\tilde{u}}{\partial\tilde{z}^2} \end{aligned} \quad (\text{A2})$$

with U as the typical scale of the M_2 tidal velocity in the longitudinal direction. The corresponding dimensionless boundary conditions at the free surface are given by

$$\tilde{w} = \frac{\partial\tilde{\eta}}{\partial\tilde{t}} + \frac{a_{M_2}}{H_0} \tilde{u} \frac{\partial\tilde{\eta}}{\partial\tilde{x}} \quad \text{and} \quad A_v \frac{\partial\tilde{u}}{\partial\tilde{z}} = 0 \quad \text{at} \quad \tilde{z} = \frac{a_{M_2}}{H_0} \tilde{\eta}. \quad (\text{A3})$$

The dimensionless boundary conditions at the bottom read

$$\tilde{w} = -\tilde{u} \frac{\partial\tilde{H}}{\partial\tilde{x}} \quad \text{and} \quad \frac{\partial\tilde{u}}{\partial\tilde{z}} = \frac{sH_0}{A_v} \tilde{u} \quad \text{at} \quad \tilde{z} = -\tilde{H}. \quad (\text{A4})$$

At the entrance of the estuary, the dimensionless boundary condition reads

$$\tilde{\eta} = \cos(\sigma\tilde{t}) \quad \text{at} \quad \tilde{x} = 0, \quad (\text{A5})$$

while at the end of estuary, it is given by

$$\int_{-\tilde{H}}^{\tilde{\eta}} \tilde{u} d\tilde{z} = \frac{R}{B_0 H_0 U} \frac{1}{\tilde{B}} \quad \text{at} \quad \tilde{x} = 1. \quad (\text{A6})$$

The dimensionless salinity equation is also derived:

$$\begin{aligned} \frac{\partial\tilde{S}}{\partial\tilde{t}} + \frac{U}{\sigma L} \tilde{u} \frac{\partial\tilde{S}}{\partial\tilde{x}} + \frac{W}{\sigma H_0} \tilde{w} \frac{\partial\tilde{S}}{\partial\tilde{z}} = \frac{K_h}{\sigma L^2} \frac{\partial}{\partial\tilde{x}} \frac{\partial\tilde{S}}{\partial\tilde{x}} + \frac{K_v}{\sigma H_0^2} \frac{\partial}{\partial\tilde{z}} \frac{\partial\tilde{S}}{\partial\tilde{z}} \\ + \frac{K_h}{\sigma L^2} \frac{1}{\tilde{B}} \frac{d\tilde{B}}{d\tilde{x}} \frac{\partial\tilde{S}}{\partial\tilde{x}}, \end{aligned} \quad (\text{A7})$$

with

$$\tilde{S} = 1 \quad \text{at} \quad \tilde{x} = 0. \quad (\text{A8})$$

This boundary condition is different from McCarthy (1993), who required no salinity gradient at the estuarine mouth. No residual salt transport is required at the weir:

$$-\int_{-\tilde{H}}^{\tilde{\eta}} \tilde{u} \tilde{S} d\tilde{z} + \frac{K_h}{UL} \int_{-\tilde{H}}^{\tilde{\eta}} \frac{\partial\tilde{S}}{\partial\tilde{x}} d\tilde{z} = 0 \quad \text{at} \quad \tilde{x} = 1, \quad (\text{A9})$$

where the overbar ($\bar{\cdot}$) means tidally averaged quantities. Moreover, no salt flux is allowed through the free surface or through the bottom:

$$K_v \frac{\partial\tilde{S}}{\partial\tilde{z}} \Big|_{\tilde{z}=\tilde{\eta}} = K_v \frac{\partial\tilde{S}}{\partial\tilde{z}} \Big|_{\tilde{z}=-\tilde{H}} = 0. \quad (\text{A10})$$

As a next step, the order of magnitudes of the above scaling parameters is provided in terms of ε for the governing equations and the boundary conditions, as summarized in Table A2. Here, $U/\sigma L = O(\varepsilon)$ follows from integrating the continuity equation over depth and requiring an approximate balance between the resulting contributions (Chernetsky et al. 2010).

Substituting the scaled variables into Eqs. (A1), (A2), and (A7) yields

TABLE A2. Order of magnitude of scaling parameters.

Dimensionless parameters	Order
a_{M_2}/H_0	$O(\varepsilon)$
$U/\sigma L = W/\sigma H_0$	$O(\varepsilon)$
$\Delta_p H_0^2 g/\rho_c U \sigma L$	$O(\varepsilon)$
$a_{M_2} g/U \sigma L$	$O(1)$
$A_v/\sigma H_0^2 = K_v/\sigma H_0^2$	$O(1)$
sH_0/A_v	$O(1)$
$R/B(L)H_0 U$	$O(\varepsilon)$
$K_h/\sigma L^2$	$O(\varepsilon^2)$
K_h/UL	$O(\varepsilon)$

$$\frac{\partial \tilde{u}}{\partial \tilde{x}} + \frac{\partial \tilde{w}}{\partial \tilde{z}} + \frac{1}{\tilde{B}} \frac{d\tilde{B}}{d\tilde{x}} \tilde{u} = 0,$$

$$\frac{\partial \tilde{u}}{\partial \tilde{t}} + \varepsilon \tilde{u} \frac{\partial \tilde{u}}{\partial \tilde{x}} + \varepsilon \tilde{w} \frac{\partial \tilde{u}}{\partial \tilde{z}} = -\varepsilon \int_{\tilde{z}}^{\tilde{\eta}} \frac{\partial \tilde{p}}{\partial \tilde{x}} d\tilde{z} - \frac{\partial \tilde{\eta}}{\partial \tilde{x}} + \frac{\partial^2 \tilde{u}}{\partial \tilde{z}^2},$$

$$\frac{\partial \tilde{S}}{\partial \tilde{t}} + \varepsilon \tilde{u} \frac{\partial \tilde{S}}{\partial \tilde{x}} + \varepsilon \tilde{w} \frac{\partial \tilde{S}}{\partial \tilde{z}} = \varepsilon^2 \frac{\partial^2 \tilde{S}}{\partial \tilde{x}^2} + \varepsilon^2 \frac{1}{\tilde{B}} \frac{d\tilde{B}}{d\tilde{x}} \frac{\partial \tilde{S}}{\partial \tilde{x}} + \frac{\partial^2 \tilde{S}}{\partial \tilde{z}^2}.$$

(A11)

The dimensionless boundary conditions in terms of ε can also be obtained using Table A2. After that, all the physical variables are expanded in power series of the ε . By substituting the expanded variables from Eq. (12) into Eqs. (A11), and their boundary conditions, and collecting the terms of the same order of ε , each system of equations of different orders of ε can be obtained.

APPENDIX B

The Leading-Order Water Motion

The leading-order dimensional equations for the water motion are

$$\frac{\partial u_0}{\partial x} + \frac{\partial w_0}{\partial z} + \frac{1}{B} \frac{dB}{dx} u_0 = 0, \quad \text{and} \quad (\text{B1})$$

$$\frac{\partial u_0}{\partial t} = -g \frac{\partial \eta_0}{\partial x} + A_v \frac{\partial^2 u_0}{\partial z^2}. \quad (\text{B2})$$

The free surface elevation is at $O(\varepsilon)$; thus, the boundary condition at the sea surface is given at $z = 0$ in the leading-order system, and hence

$$w_0 = \frac{\partial \eta_0}{\partial t} \quad \text{and} \quad A_v \frac{\partial u_0}{\partial z} = 0,$$

and at the bottom ($z = -H$)

$$w_0 = -u_0 \frac{dH}{dx} \quad \text{and} \quad A_v \frac{\partial u_0}{\partial z} = s u_0.$$

The leading-order system is forced by a M_2 tide at the entrance,

$$\eta_0 = a_{M_2} \cos(\sigma t),$$

and no water transport in the leading order is allowed at the end of estuary ($x = L$):

$$\int_{-H}^0 u_0 dz = 0.$$

The leading-order hydrodynamic system allows solutions of the following form:

$$(u_0, w_0, \eta_0) = \Re[\hat{u}_0(x, z), \hat{w}_0(x, z), \hat{\eta}_0(x) e^{i\sigma t}], \quad (\text{B3})$$

where \Re means only the real parts of the solutions are used, and \hat{u}_0 , \hat{w}_0 , and $\hat{\eta}_0$ are the complex amplitudes of u_0 , w_0 , and η_0 , respectively. Substituting Eq. (B3) into Eqs. (B1) and (B2) yields

$$\frac{\partial \hat{u}_0}{\partial x} + \frac{\partial \hat{w}_0}{\partial z} + \frac{1}{B} \frac{dB}{dx} \hat{u}_0 = 0, \quad \text{and} \quad (\text{B4})$$

$$i\sigma \hat{u}_0 + g \frac{d\hat{\eta}_0}{dx} - A_v \frac{\partial^2 \hat{u}_0}{\partial z^2} = 0. \quad (\text{B5})$$

Solving Eq. (B5) using the corresponding boundary conditions regarding u_0 yields

$$\hat{u}_0 = \frac{g}{i\sigma} \frac{d\hat{\eta}_0}{dx} \left(\alpha \cosh \delta \frac{z}{H} - 1 \right), \quad (\text{B6})$$

$$\text{with } \delta = \frac{1+i}{\text{Stk}}, \quad \text{and } \alpha = \left(\cosh \delta + \frac{A_v}{sH} \delta \sinh \delta \right)^{-1}. \quad (\text{B7})$$

Here, $\text{Stk} = \sqrt{2A_v/\sigma}/H$ is the Stokes number.

By substituting Eq. (B6) into Eq. (B4), and applying the boundary conditions regarding w_0 , we derive a second-order ordinary differential equation:

$$\begin{aligned} T_1(x) \frac{d^2 \hat{\eta}_0}{dx^2} - T_2(x) \frac{d\hat{\eta}_0}{dx} - T_3(x) \hat{\eta}_0 &= 0, \quad \text{with } T_1(x) = \frac{\alpha \sinh \delta - \delta}{\delta} H, \\ T_2(x) &= -\frac{1}{B} \frac{dB}{dx} T_1(x) - \frac{\sinh \delta}{\delta} \frac{d\alpha}{dx} H - (\alpha \cosh \delta - 1) \frac{dH}{dx}, \\ T_3(x) &= \frac{\sigma^2}{g}. \end{aligned} \quad (\text{B8})$$

Equation (B8) can be solved together with the boundary conditions of η_0 . Note that T_1 and T_2 are functions of x for a spatially varying bathymetry; thus, a finite-difference method is used to obtain $\hat{\eta}_0$ for a depth-varying estuary. In this sense, the model is solved semianalytically.

However, Eq. (B8) can be solved analytically for estuaries with a horizontal bed and an exponentially converging width [see Eq. (22)]. The analytical solutions of the sea surface elevation and the longitudinal sea surface gradient read

$$\hat{\eta}_0 = \frac{a_{M_2} e^{x/(2L_b)} \left\{ -\sinh \left[\frac{k}{2}(x-L) \right] + L_b k \cosh \left[\frac{k}{2}(x-L) \right] \right\}}{\sinh \left(\frac{kL}{2} \right) + kL_b \cosh \left(\frac{kL}{2} \right)}, \quad \text{and} \quad (B9)$$

$$\frac{d\hat{\eta}_0}{dx} = \frac{a_{M_2} e^{x/(2L_b)} \sinh \left[\frac{k}{2}(x-L) \right] \left(-\frac{1}{2L_b} + \frac{k^2 L_b}{2} \right)}{\sinh \left(\frac{kL}{2} \right) + kL_b \cosh \left(\frac{kL}{2} \right)}, \quad (B10)$$

with $k = \sqrt{1/L_b^2 + 4\sigma^2\delta/[gH(\alpha \sinh\delta - \delta)]}$ as the complex wavenumber.

This means that the correct expressions are obtained by replacing $\rho'_0(x)$ with $\Re[\rho'_0(x)]$, that is, by taking $\rho_0(x)$ to be real. Substituting Eq. (C2) into Eq. (C1) gives

APPENDIX C

The Analytical Solution for Salinity

The dimensional salinity equation in the first order is

$$\frac{\partial S_1}{\partial t} + u_0 \frac{\partial S_0}{\partial x} = K_v \frac{\partial^2 S_1}{\partial z^2}, \quad (C1)$$

with

$$S_1 = \Re(\hat{S}_1 e^{i\sigma t}). \quad (C2)$$

The leading-order salinity S_0 is taken to be real. Note that this is different from McCarthy (1993), who allows the leading-order density to be complex, resulting in an incorrect expression for density [see Eq. (19) in McCarthy (1993)]. The correct expression reads

$$\rho_1 = \Re\{A'(x)\rho(z)\Re[\rho'_0(x)]e^{i\sigma t}\}.$$

Hence, it was erroneously assumed by McCarthy (1993) that

$$\Re\{u_0 \Re[\rho'_0(x)]\} = \Re\{\hat{u}_0 \rho'_0(x) e^{i\sigma t}\},$$

whereas it is equal to

$$\Re\{\hat{u}_0 e^{i\sigma t} \Re[\rho'_0(x)]\}.$$

$$i\sigma \hat{S}_1 + \hat{u}_0 \frac{\partial S_0}{\partial x} = K_v \frac{\partial^2 \hat{S}_1}{\partial z^2}. \quad (C3)$$

As u_0 can be solved independently of salinity [see Eq. (B6)], it can be written as

$$\hat{u}_0 = U(x, z) \frac{g}{i\sigma} \frac{d\hat{\eta}_0}{dx}, \quad \text{with} \quad U(x, z) = \alpha \cosh\delta \frac{z}{H} - 1. \quad (C4)$$

Equation (C3) suggests S_1 can be written as

$$\hat{S}_1 = S_z(x, z) \frac{d\hat{\eta}_0}{dx} \frac{dS_0}{dx}. \quad (C5)$$

The term S_z measures how the vertical structure of the tidal salinity is influenced by the vertical profile of the tidal velocity, and it relates the gradients of the tidal elevation and subtidal salinity with the tidal salinity. Substituting Eqs. (C4) and (C5) into Eq. (C3) yields

$$\frac{\partial^2 S_z}{\partial z^2} - \frac{i\sigma}{K_v} S_z = \frac{ig}{K_v \sigma} \left(1 - \alpha \cosh\delta \frac{z}{H} \right). \quad (C6)$$

Notice that the no salt flux through the free surface and the bottom is equivalent to a zero vertical gradient of S_z :

$$\left. \frac{\partial S_z}{\partial z} \right|_{z=0} = \left. \frac{\partial S_z}{\partial z} \right|_{z=-H} = 0. \quad (C7)$$

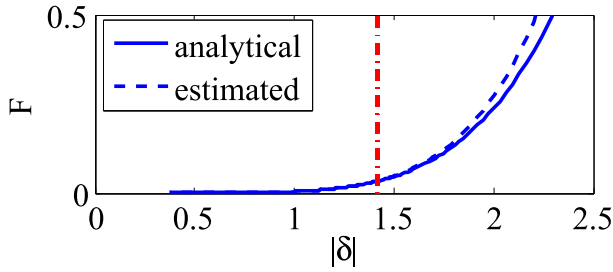


FIG. D1. The comparison of the analytical solution of F (solid blue line) with the estimated F using Eq. (D6) (dashed blue line). The red dashed-dotted line represents the absolute value of $|\delta| = \sqrt{2}$.

Using Eqs. (C6) and (C7), $S_z(x, z)$ can be solved analytically for estuaries of any bathymetry $H(x)$. The analytical solution reads

$$S_z(x, z) = \frac{g}{\sigma^2} \left[-1 + \frac{\alpha}{2} \left(1 + \delta \frac{\cosh \delta}{\sinh \delta} \right) \cosh \delta \frac{z}{H} - \frac{\alpha}{2} \delta \frac{z}{H} \sinh \delta \frac{z}{H} \right]. \quad (\text{C8})$$

APPENDIX D

The Estimation of K_h^{adv}

To derive an estimate of K_h^{adv} , the complex amplitudes of the M_2 tidal velocity \hat{u}_0 and salinity \hat{S}_1 are decomposed into a depth-averaged part and the deviation from this depth average:

$$\hat{u}_0 = \langle \hat{u}_0(x) \rangle + \hat{u}'_0(x, z), \quad \text{and} \quad (\text{D1})$$

$$\hat{S}_1 = \langle \hat{S}_1(x) \rangle + \hat{S}'_1(x, z). \quad (\text{D2})$$

Here, $\langle \cdot \rangle$ means averaging over depth, and the prime indicates the deviation from the depth average.

$$F = -\frac{1}{H} \int_{-H}^0 \left[\cosh\left(\frac{\delta z}{H}\right) - \frac{\sinh(\delta)}{\delta} \right] \left\{ \cosh\left(\frac{\delta z}{H}\right) \left[1 + \delta \frac{\cosh(\delta)}{\sinh(\delta)} \right] - \frac{\delta z}{H} \sinh\left(\frac{\delta z}{H}\right) - 2 \frac{\sinh(\delta)}{\delta} \right\} dz. \quad (\text{D5})$$

Since F depends only on δ for a given H , and $|\delta|$ is small for well-mixed estuaries, it yields an estimation of F after using the Taylor expansion:

$$F \approx \frac{32}{945} \text{Stk}^{-6}. \quad (\text{D6})$$

As pointed out by Souza (2013), that boundary layer increases with Stk , and it covers the entire water column (estuary being well mixed) when Stk approaches unity. Hence, the well-mixed assumption

Averaging Eq. (14) over depth using the boundary condition from Eq. (11) shows that the depth-averaged M_2 salinity is 90° out of phase with the depth-averaged tidal velocity. This implies that the tidal advective diffusivity only results from the correlation between the depth-varying parts of the tidal velocity and salinity. Then, \hat{u}'_0 and $\hat{S}'_1/(dS_0/dx)$ [used in Eq. (19)] are written in terms of $\hat{\eta}_0$ and S_0 (see appendixes B and C for details):

$$\hat{u}'_0 = \frac{g\alpha}{i\sigma} \frac{d\hat{\eta}_0}{dx} \left[\cosh\left(\frac{\delta z}{H}\right) - \frac{\sinh(\delta)}{\delta} \right],$$

$$\hat{S}'_1 = \frac{g\alpha}{2\sigma^2} \frac{d\hat{\eta}_0}{dx} \frac{dS_0}{dx} \left\{ \left[1 + \delta \frac{\cosh(\delta)}{\sinh(\delta)} \right] \cosh\left(\frac{\delta z}{H}\right) - \frac{\delta z}{H} \sinh\left(\frac{\delta z}{H}\right) - 2 \frac{\sinh(\delta)}{\delta} \right\},$$

with $\delta = (1 + i)/\text{Stk}$. Here,

$$\text{Stk} = \sqrt{\frac{2A_v}{\sigma H^2}}$$

is the Stokes number. The parameter α depends on both δ and the dimensionless partial-slip parameter s^* ($=s/\sigma H$) and is given by

$$\alpha = \left[\cosh(\delta) + \frac{i}{\delta s^*} \sinh(\delta) \right]^{-1}. \quad (\text{D3})$$

Hence, K_h^{adv} can be analytically solved using only the M_2 tidal motion, as

$$K_h^{\text{adv}} = \frac{1}{4} \frac{g^2}{\sigma^3} \left| \frac{d\hat{\eta}_0}{dx} \right|^2 |\alpha|^2 F, \quad (\text{D4})$$

where F is the vertical integral given by

has to be valid when $|\delta|$ ($=\sqrt{2}/\text{Stk}$) is smaller than $\sqrt{2}$. Figure D1 shows that the estimated F using Eq. (D6) agrees well with the analytical results obtained from Eq. (D5). It means that Eq. (D6) is a good estimate of F for well-mixed estuaries. Substituting Eq. (D6) into Eq. (D4) yields an estimate of the tidal advective diffusivity:

$$K_h^{\text{adv}} \approx \frac{8}{945} \frac{g^2}{\sigma^3} \left| \frac{d\hat{\eta}_0}{dx} \right|^2 \frac{1}{\text{Stk}^6}. \quad (\text{D7})$$

REFERENCES

- Aristizábal, M., and R. Chant, 2013: A numerical study of salt fluxes in Delaware Bay estuary. *J. Phys. Oceanogr.*, **43**, 1572–1588, doi:10.1175/JPO-D-12-0124.1.
- Bowen, M. M., and W. R. Geyer, 2003: Salt transport and the time-dependent salt balance of a partially stratified estuary. *J. Geophys. Res.*, **108**, 3158, doi:10.1029/2001JC001231.
- Burchard, H., and H. Baumert, 1998: The formation of estuarine turbidity maxima due to density effects in the salt wedge. A hydrodynamic process study. *J. Phys. Oceanogr.*, **28**, 309–321, doi:10.1175/1520-0485(1998)028<0309:TFOETM>2.0.CO;2.
- , and R. D. Hetland, 2010: Quantifying the contributions of tidal straining and gravitational circulation to residual circulation in periodically stratified tidal estuaries. *J. Phys. Oceanogr.*, **40**, 1243–1262, doi:10.1175/2010JPO4270.1.
- , —, E. Schulz, and H. M. Schuttelaars, 2011: Drivers of residual estuarine circulation in tidally energetic estuaries: Straight and irrotational channels with parabolic cross section. *J. Phys. Oceanogr.*, **41**, 548–570, doi:10.1175/2010JPO4453.1.
- Cheng, P., A. Valle-Levinson, and H. E. De Swart, 2010: Residual currents induced by asymmetric tidal mixing in weakly stratified narrow estuaries. *J. Phys. Oceanogr.*, **40**, 2135–2147, doi:10.1175/2010JPO4314.1.
- Chernetsky, A. S., H. M. Schuttelaars, and S. A. Talke, 2010: The effect of tidal asymmetry and temporal settling lag on sediment trapping in tidal estuaries. *Ocean Dyn.*, **60**, 1219–1241, doi:10.1007/s10236-010-0329-8.
- Davies, A., and J. Jones, 1996: Sensitivity of tidal bed stress distributions, near-bed currents, overtides, and tidal residuals to frictional effect in the eastern Irish Sea. *J. Phys. Oceanogr.*, **26**, 2553–2575, doi:10.1175/1520-0485(1996)026<2553:SOTBSD>2.0.CO;2.
- Fischer, H., 1972: Mass transport mechanisms in partially stratified estuaries. *J. Fluid Mech.*, **53**, 671–687, doi:10.1017/S0022112072000412.
- Friedrichs, C. T., and D. G. Aubrey, 1994: Tidal propagation in strongly convergent channels. *J. Geophys. Res.*, **99**, 3321–3336, doi:10.1029/93JC03219.
- Garvine, R. W., R. K. McCarthy, and K.-C. Wong, 1992: The axial salinity distribution in the Delaware estuary and its weak response to river discharge. *Estuarine Coastal Shelf Sci.*, **35**, 157–165, doi:10.1016/S0272-7714(05)80110-6.
- Geyer, W. R., and P. MacCready, 2014: The estuarine circulation. *Annu. Rev. Fluid Mech.*, **46**, 175–197, doi:10.1146/annurev-fluid-010313-141302.
- Giese, B., and D. Jay, 1989: Modelling tidal energetics of the Columbia River estuary. *Estuarine Coastal Shelf Sci.*, **29**, 549–571, doi:10.1016/0272-7714(89)90010-3.
- Hansen, D. V., and M. Rattray Jr., 1965: Gravitational circulation in straits and estuaries. *J. Mar. Res.*, **23**, 104–122.
- Hughes, F., and M. Rattray Jr., 1980: Salt flux and mixing in the Columbia River estuary. *Estuarine Coastal Mar. Sci.*, **10**, 479–493, doi:10.1016/S0302-3524(80)80070-3.
- Ianniello, J. P., 1979: Tidally induced residual currents in estuaries of variable breadth and depth. *J. Phys. Oceanogr.*, **9**, 962–974, doi:10.1175/1520-0485(1979)009<0962:TIRCIE>2.0.CO;2.
- Jay, D. A., and J. D. Smith, 1990a: Residual circulation in shallow estuaries: 1. Highly stratified, narrow estuaries. *J. Geophys. Res.*, **95**, 711–731, doi:10.1029/JC095iC01p00711.
- , and —, 1990b: Residual circulation in shallow estuaries: 2. Weakly stratified and partially mixed systems. *J. Geophys. Res.*, **95**, 733–748, doi:10.1029/JC095iC01p00733.
- , and —, 1990c: Circulation, density distribution and neap-spring transitions in the Columbia River estuary. *Prog. Oceanogr.*, **25**, 81–112, doi:10.1016/0079-6611(90)90004-L.
- Jones, J., and A. Davies, 1996: A high-resolution, three-dimensional model of the M₂, M₄, M₆, S₂, N₂, K₁ and O₁ tides in the eastern Irish Sea. *Estuarine Coastal Shelf Sci.*, **42**, 311–346, doi:10.1006/ecss.1996.0022.
- Kjerfve, B., 1986: Circulation and salt flux in a well mixed estuary. *Physics of Shallow Estuaries and Bays*, J. van de Kreeke, Ed., Lecture Notes on Coastal and Estuarine Studies Series, Vol. 16, Amer. Geophys. Union, 22–29.
- Kuijper, K., and L. C. Van Rijn, 2011: Analytical and numerical analysis of tides and salinities in estuaries; Part II: Salinity distributions in prismatic and convergent tidal channels. *Ocean Dyn.*, **61**, 1743–1765, doi:10.1007/s10236-011-0454-z.
- Lanzoni, S., and G. Seminara, 1998: On tide propagation in convergent estuaries. *J. Geophys. Res.*, **103**, 30 793–30 812, doi:10.1029/1998JC900015.
- Lerczak, J. A., W. R. Geyer, and R. J. Chant, 2006: Mechanisms driving the time-dependent salt flux in a partially stratified estuary. *J. Phys. Oceanogr.*, **36**, 2296–2311, doi:10.1175/JPO2959.1.
- MacCready, P., 2004: Toward a unified theory of tidally-averaged estuarine salinity structure. *Estuaries*, **27**, 561–570, doi:10.1007/BF02907644.
- , and W. R. Geyer, 2010: Advances in estuarine physics. *Annu. Rev. Mar. Sci.*, **2**, 35–58, doi:10.1146/annurev-marine-120308-081015.
- McCarthy, R. K., 1993: Residual currents in tidally dominated, well-mixed estuaries. *Tellus*, **45A**, 325–340, doi:10.1034/j.1600-0870.1993.00007.x.
- Peters, J., and R. Wollast, 1976: Role of the sedimentation in the self-purification of the Scheldt estuary. *Proc. Third Federal Interagency Sedimentation Conf.*, Denver, CO, Water Resources Council, 3-77–3-82.
- Prandle, D., 2003: Relationships between tidal dynamics and bathymetry in strongly convergent estuaries. *J. Phys. Oceanogr.*, **33**, 2738–2750, doi:10.1175/1520-0485(2003)033<2738:RBTDAB>2.0.CO;2.
- Rattray, M., and J. Dworski, 1980: Comparison of methods for analysis of the transverse and vertical circulation contributions to the longitudinal advective salt flux in estuaries. *Estuarine Coastal Mar. Sci.*, **11**, 515–536, doi:10.1016/S0302-3524(80)80004-1.
- Savenije, H. H., 1993: Composition and driving mechanisms of longitudinal tidal average salinity dispersion in estuaries. *J. Hydrol.*, **144**, 127–141, doi:10.1016/0022-1694(93)90168-9.
- , 2012: *Salinity and Tides in Alluvial Estuaries*. 2nd ed. Savenije, 163 pp. [Available online at <https://salinityandtides.com/>.]
- , and E. J. Veling, 2005: Relation between tidal damping and wave celerity in estuaries. *J. Geophys. Res.*, **110**, C04007, doi:10.1029/2004JC002278.
- Schramkowski, G. P., and H. de Swart, 2002: Morphodynamic equilibrium in straight tidal channels: Combined effects of Coriolis force and external overtides. *J. Geophys. Res.*, **107**, 3227, doi:10.1029/2000JC000693.
- , —, and H. M. Schuttelaars, 2010: Effect of bottom stress formulation on modelled flow and turbidity maxima in cross-sections of tide-dominated estuaries. *Ocean Dyn.*, **60**, 205–218, doi:10.1007/s10236-009-0235-0.
- Souza, A., 2013: On the use of the Stokes number to explain frictional tidal dynamics and water column structure in shelf seas. *Ocean Sci.*, **9**, 391–398, doi:10.5194/os-9-391-2013.
- Taylor, G., 1953: Dispersion of soluble matter in solvent flowing slowly through a tube. *Proc. Roy. Soc. London*, **A219**, 186–203, doi:10.1098/rspa.1953.0139.
- , 1954: The dispersion of matter in turbulent flow through a pipe. *Proc. Roy. Soc. London*, **A223**, 446–468, doi:10.1098/rspa.1954.0130.